

# TDBENCH: A BENCHMARK FOR TOP-DOWN IMAGE UNDERSTANDING WITH RELIABILITY ANALYSIS OF VISION-LANGUAGE MODELS

**Kaiyuan Hou\***, **Minghui Zhao\***, **Lilin Xu**, **Yuang Fan** & **Xiaofan Jiang**

Department of Electrical Engineering

Columbia University

{kh3119,mz2869,lx2331,yf2676}@columbia.edu, jiang@ee.columbia.edu

## ABSTRACT

Top-down images play an important role in safety-critical settings such as autonomous navigation and aerial surveillance, where they provide holistic spatial information that front-view images cannot capture. Despite this, Vision Language Models (VLMs) are mostly trained and evaluated on front-view benchmarks, leaving their performance in the top-down setting poorly understood. Existing evaluations also overlook a unique property of top-down images: their physical meaning is preserved under rotation. In addition, conventional accuracy metrics can be misleading, since they are often inflated by hallucinations or “lucky guesses”, which obscures a model’s true reliability and its grounding in visual evidence. To address these issues, we introduce TDBench, a benchmark for top-down image understanding that includes 2000 curated questions for each rotation. We further propose RotationalEval (RE), which measures whether models provide consistent answers across four rotated views of the same scene, and we develop a reliability framework that separates genuine knowledge from chance. Finally, we conduct four case studies targeting underexplored real-world challenges. By combining rigorous evaluation with reliability metrics, TDBench not only benchmarks VLMs in top-down perception but also provides a new perspective on trustworthiness, guiding the development of more robust and grounded AI systems.<sup>1</sup>

## 1 INTRODUCTION

Top-down images provide comprehensive spatial overviews and clear geometric context, supporting tasks such as autonomous navigation, aerial surveillance, mapping, and disaster assessment (Lu et al., 2018; Nearmap, 2022; Zhao et al., 2025). Top-down images from drones or satellites provide a complete “bird’s-eye” view, offering several unique advantages over conventional front-view images: they reduce occlusion between objects, maintain more consistent scale across the frame, and reveal complete spatial layouts that are impossible to observe from ground level. These properties allow analysts or autonomous systems to reason about large geographic areas efficiently, which is essential in applications such as traffic monitoring, urban planning, and environmental response.

Despite their importance, top-down images are substantially underrepresented in the datasets commonly used to train and evaluate Vision Language Models (VLMs). Well-known datasets such as COCO (Lin et al., 2015) and ImageNet (Russakovsky et al., 2015) contain primarily front-view images, where appearance cues, object sizes, and spatial relationships are largely different from aerial perspectives. For instance, in our preliminary data audit, fewer than 7% images (595 of 8,629) from the VisDrone dataset (Zhu et al., 2021) could be considered truly top-down. This limited coverage leaves current VLMs largely untested for top-down understanding, even though such models are increasingly applied in drone-based and remote-sensing systems.

Most existing VLM benchmarks (Liu et al., 2024b; Yue et al., 2024; Yu et al., 2024; Lu et al., 2024) are not designed for top-down images. While these benchmarks have driven progress in general-purpose

\*These authors contributed equally to this work

<sup>1</sup>Project website: <https://github.com/Columbia-ICSL/TDBench>

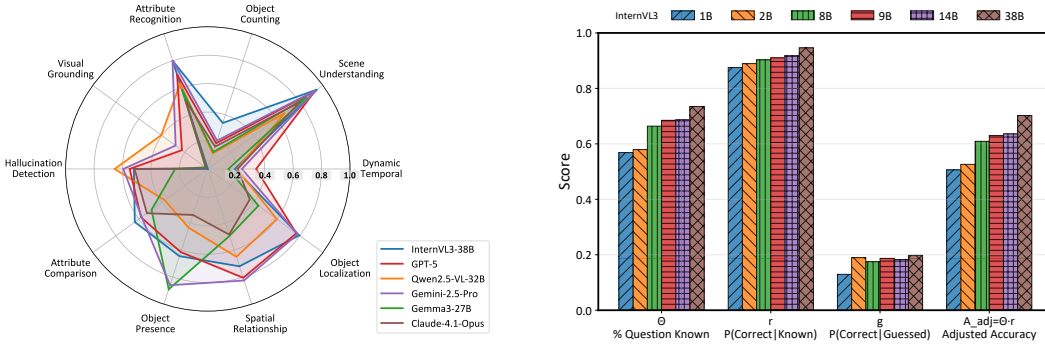


Figure 1: **(Left)** Accuracy across ten top-down image tasks in TDBench. **(Right)** Knowledge decomposition analysis from TDBench: % of questions known ( $\theta$ ) measures the proportion of questions a model truly knows;  $P(\text{Correct}|\text{Known})$  ( $r$ ) is the model’s accuracy among the questions that it knows;  $P(\text{Correct}|\text{Guessed})$  ( $g$ ) is the model’s accuracy among the questions it does not know; and the Adjusted Accuracy ( $A_{adj} = \theta \cdot r$ ) is the model’s accuracy without lucky guesses.

visual reasoning, they provide little insight into how VLMs handle the distinct challenges of top-down perception. Aerial scenes present small, densely packed objects, drastically different viewing angles, and weak perspective depth cues. Contextual cues that aid object recognition in conventional images may be absent or transformed in top-down perspectives. VLMs trained mostly on canonical-view data often fail to generalize to these conditions, leading to severe accuracy drops (Danish et al., 2025; Li et al., 2024a). Without a dedicated benchmark, it is difficult to measure or systematically improve their performance on top-down views.

To address this gap, we present TDBench, a benchmark for evaluating VLMs on top-down image understanding. TDBench contains 2,000 carefully constructed questions drawn from public aerial datasets and high-fidelity simulations, covering diverse settings and tasks relevant to real-world operations. We also introduce RotationalEval (RE), an evaluation method that leverages a key property of top-down images: their physical meaning is preserved under rotation. Unlike front-view images, where rotation produces implausible scenes (for example, the sky appearing below or objects upside down), rotating a top-down image is equivalent to changing a drone’s heading, so the scene remains physically consistent. RE tests whether models can answer correctly across all four rotated views, recognizing that semantics and object identities remain the same while spatial descriptors (e.g., “top-left”), and coordinates legitimately change. This provides a stricter and more diagnostic measure of visual reasoning, reducing the influence of spurious one-off successes.

Vision Language Models (VLMs) often hallucinate, generating answers from learned text patterns instead of grounding them in the provided image (Li et al., 2023b; Bai et al., 2025b). This can artificially inflate scores under conventional evaluation. However, an ungrounded guess is highly unlikely to be correct across four different rotations, RE naturally filters out these successes. We further formalize this with new reliability-oriented metrics that disentangle a model’s visually-grounded knowledge from its apparent accuracy. This provides a more quantitative view of model trustworthiness than raw accuracy alone.

Finally, we conduct four application-oriented case studies for real-world applications: digital and physical “zoom-in”, handling partially visible objects and reasoning about depth from 2D views. These case studies demonstrate how TDBench can guide the design and deployment of VLM-based aerial systems. In summary, our main contributions are:

- **Application-driven Benchmark.** We build TDBench, a top-down benchmark of **2,000** question-answer pairs from public datasets and high-fidelity simulation, organized into ten evaluation dimensions. To demonstrate its practical relevance, we also conduct **four case studies** that examine VLMs on real-world aerial applications, providing actionable insights for deployment.
- **Rotation-invariant Evaluation.** We introduce **RotationalEval (RE)**, an evaluation strategy that requires consistent answers across four rotated views of each image. By requiring models to be rotationally consistent, correctly adapting their spatial reasoning to each orientation, RE provides a far more robust and diagnostic measure of their performance than single-view evaluation.

- 
- **Probability-based Knowledge Reliability Analysis.** Beyond raw and RE accuracy, we propose a **probabilistic analysis** that decomposes model performance into *% of questions known* ( $\theta$ ),  $P(\text{Correct}|\text{Known})$  ( $r$ ),  $P(\text{Correct}|\text{Guessed})$  ( $g$ ), and further aggregate them into *Adjusted Accuracy* ( $\theta \cdot r$ ), which reveals how much of a model’s apparent correctness stems from genuine knowledge rather than lucky guesses.

## 2 RELATED WORKS

### 2.1 VISION LANGUAGE MODELS (VLMs)

Vision Language Models (VLMs) extend large language models (LLMs) to visual inputs by aligning image features with text representations. Most current VLMs adopt a two-stage design: a pretrained visual encoder (e.g., CLIP (Radford et al., 2021) or SigLIP (Zhai et al., 2023)) is coupled with a pretrained text-only LLM via a learnable projection module, as in LLaVA (Li et al., 2024b) and InternVL (Chen et al., 2025). This setup preserves the language backbone while enabling it to interpret visual features. Some models instead use early-fusion architectures that train perception and language components jointly, strengthening visual grounding and cross-modal reasoning. Proprietary models such as GPT (OpenAI, 2024), Gemini (Google, 2024), and Claude (Anthropic, 2024) may follow similar multimodal principles at larger scales.

VLMs are generally trained on large-scale image–text pairs from datasets like LAION (Schuhmann et al., 2022), COCO (Lin et al., 2015), and ImageNet (Russakovsky et al., 2015), which may contain few top-down images and thus treat them as out-of-distribution (OOD). While this broad training enables rich visual–linguistic knowledge, it biases models toward ground-level scenes and object appearances. As a result, their generalization to top-down views, where objects appear smaller, depth cues are weak, and spatial relationships dominate, remains underexplored, motivating the need for a dedicated benchmark.

### 2.2 VLM BENCHMARKS

Recent years have seen the emergence of numerous benchmarks for evaluating Vision–Language Models (VLMs) on diverse multimodal reasoning tasks. General-purpose benchmarks such as MMBench (Liu et al., 2024b), MMMU (Yue et al., 2024), MME (Fu et al., 2024), and MM-Vet (Yu et al., 2024) assess general knowledge, visual perception, commonsense reasoning, and spatial understanding. However, these benchmarks focus primarily on conventional front-view imagery and include few tasks involving aerial or top-down perspectives. They thus overlook challenges unique to top-down understanding, including extreme scale variation, weak depth cues, and dense spatial layouts, which often cause VLMs to underperform on aerial tasks.

A few recent efforts have begun addressing this gap using remote sensing images. For example, Hu et al. (2023), Muhtar et al. (2024), Kuckreja et al. (2023), and Danish et al. (2025) evaluate VLMs on satellite data. These datasets mostly comprise low-resolution images (meters per pixel) aimed at large-scale land cover classification or scene categorization. They rarely involve human-scale and near-surface views tasks such as object localization, attribute comparison, or spatio-temporal analysis. Moreover, satellite images are typically captured from fixed nadir viewpoints at consistent altitudes, lacking the perspective variation and dynamic conditions common in drone operations.

Beyond remote sensing, only a few studies explore top-down images. For instance, Li et al. (2024a) introduces an indoor map benchmark for evaluating navigation and spatial reasoning from floor plans. In contrast, our benchmark TDBench focuses on high-resolution, near-surface top-down images resembling drone viewpoints, enabling systematic evaluation of fine-grained perception and reasoning abilities that remain underrepresented in existing benchmarks.

### 2.3 HALLUCINATIONS IN MULTIMODAL LLMs

Hallucination has become an increasing concern in both large language models (LLMs) and vision–language models (VLMs). In VLMs, it often occurs when models generate content that is inconsistent with the image, such as describing nonexistent objects, misrepresenting spatial relationships, or ignoring the visual input entirely (Wang et al., 2024). Recent studies have introduced

---

benchmarks and methods to systematically evaluate these visual hallucinations. Li et al. (2023a) introduced the POPE method, which probes object hallucination by asking targeted presence/absence questions and measuring how often models falsely claim the existence of unseen objects. Liu et al. (2024a) provided a large-scale study on hallucinations in VLMs and proposed automatic detection metrics based on grounding scores, which assess alignment between textual output and visual evidence. HallusionBench (Guan et al., 2024) proposed a diagnostic benchmark designed to isolate hallucination behavior using paired, contrastive visual questions to reveal when models invent objects or attributes.

These approaches typically rely on comparing generated captions or answers against ground-truth annotations, using measures such as hallucination rate (percentage of fabricated objects), grounding accuracy (percentage of correctly grounded mentions), or contrastive consistency scores. However, current methods primarily treat hallucination as a binary outcome (hallucinated or correct) and do not assess whether correct answers arise from genuine visual understanding or from chance agreement with priors. Our benchmark TDBench complements these efforts by a reliability-oriented evaluation perspective, aiming to distinguish reliably grounded responses from lucky successes.

### 3 DESIGN OF TDBENCH

In this section, we provide an overview of the 10 categories in TDBench with examples in Figure 2. We then describe the data sources used to build the benchmark and the procedures for curating and annotating the dataset.

#### 3.1 ABILITY TAXONOMY OF TDBENCH

TDBench evaluates top-down image understanding across 10 categories, as illustrated in Figure 1 (Left). These categories are derived from common aerial tasks in real-world applications. To ensure the benchmark targets perspective-sensitive capabilities, we excluded evaluation dimensions that are already well covered in existing benchmarks or that remain largely unaffected by viewpoint changes, such as text recognition or general knowledge recall. Broadly, the categories can be grouped into three types:

**Image Perception** This category focuses on the broad-scale interpretation of top-down aerial imagery, emphasizing holistic semantic understanding rather than fine-grained details. Such capabilities are especially valuable for wide-area reconnaissance, where drones must scan large regions to detect critical features such as wildfire outbreaks, traffic congestion, or emergency response scenarios. It includes two tasks: *Scene Understanding*, which evaluates a model’s ability to comprehend the overall contextual meaning of a scene, and *Hallucination Detection*, which assesses its ability to distinguish actual image content from fabricated choices. These tasks are shown in **blue** in Figure 2 and represent foundational abilities for reliable aerial image interpretation.

**Single-Instance Understanding** This category emphasizes detailed object-level recognition and localization within a single image, as shown in **green** in Figure 2. It covers both recognition and localization aspects. For recognition, *Object Presence* evaluates basic detection capabilities, and *Attribute Recognition* assesses the identification of specific properties such as color, shape, material, or species. For localization, we use a three-tiered approach: coarse presence detection (*Object Presence*), intermediate 3×3 grid-based localization (*Object Localization*) requiring quadrant-level precision, and fine-grained *Visual Grounding* using exact bounding box coordinates. We also include *Object Counting* to assess quantification abilities, which is particularly challenging in aerial contexts where many similar objects appear at varying scales and densities.

**Multi-Instance Reasoning** This category evaluates compositional reasoning across multiple objects, requiring analysis of spatial, comparative, and temporal relationships, as shown in **yellow** in Figure 2. *Spatial Relationship* tasks challenge models to localize multiple objects and accurately determine their relative positions, which is crucial for navigation and path planning in autonomous aerial systems. *Attribute Comparison* requires models to compare properties or states across multiple entities, useful for anomaly detection and identifying distinctive features. Finally, *Dynamic Temporal*

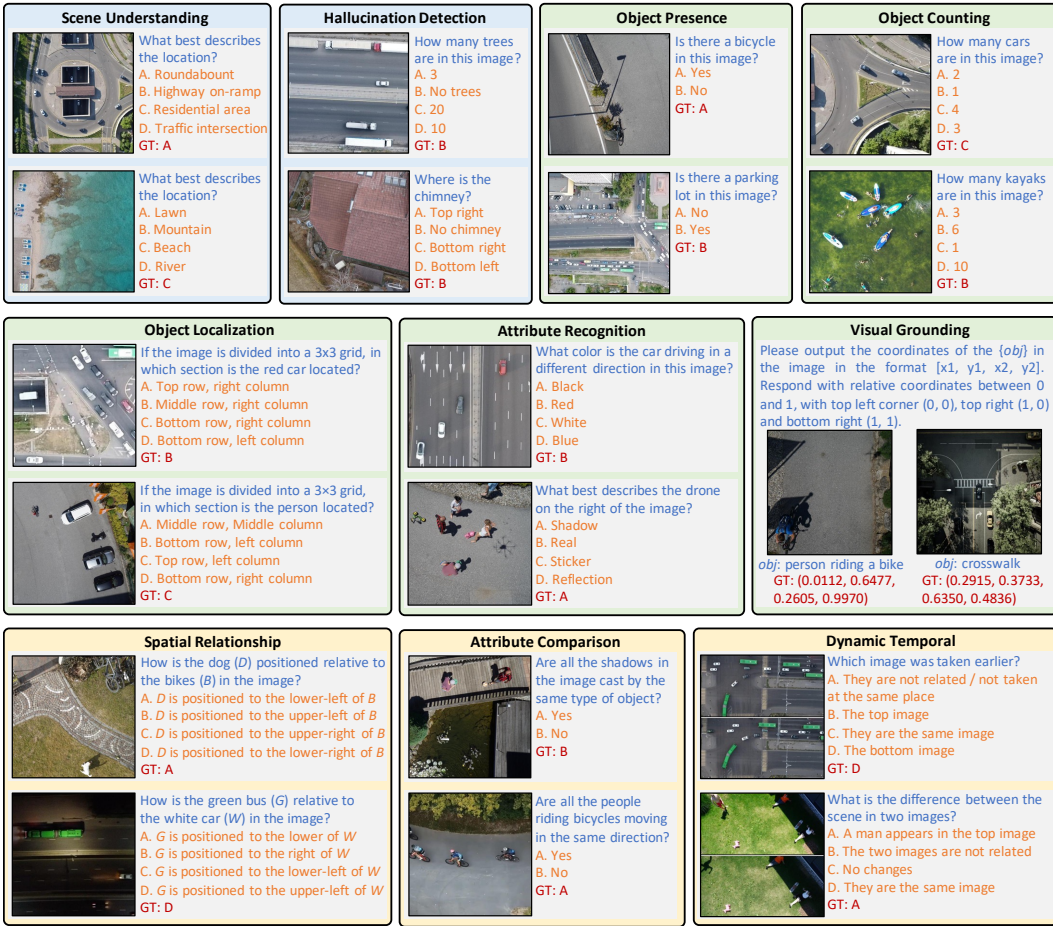


Figure 2: Benchmark examples across the ten categories in TDBench. Different colors indicate the three high-level capability groups: image perception (blue), single-instance understanding (green), and multi-instance reasoning (yellow). ‘GT’ refers to ground truth.

presents pairs of images to evaluate models’ ability to detect changes, reason about temporal order, and infer causal relationships.

### 3.2 TDBENCH CONSTRUCTION

#### 3.2.1 DATA SOURCES

We constructed TDBench from two primary sources: curated public datasets (Shaha, 2025; Zhu et al., 2021; Gasienica-Jozkowy et al., 2021; ICG, 2019; Varga et al., 2022; Mou et al., in press) and realistic simulation (CARLA Simulator (Dosovitskiy et al., 2017) and GTA V ) covering varied environments, including urban infrastructure, remote wilderness, and disaster zones (Table 1). All images from these datasets were manually selected and annotated following our evaluation taxonomy. In addition to real-world data, we generated synthetic images using the CARLA simulator with custom scripts to control scene parameters precisely. For specialized case studies requiring exact ground truth, such as camera altitude, object counts, or height measurements, we used both CARLA and *Grand Theft Auto V* (GTA V).

**CARLA Simulation** CARLA (Dosovitskiy et al., 2017) is an open-source autonomous driving simulator that provides high-fidelity urban environments and physics. We used its configurable RGB and segmentation cameras at various altitudes to generate synthetic data. This setup enables precise

Table 1: Distribution of data sources in TDBench

Image Source	Problem Formulation	Number	Ratio
Aerial Traffic Images (Shaha, 2025)	Human Annotation	<b>457</b>	20.8%
Semantic Drone (ICG, 2019)	Human Annotation	<b>653</b>	29.7%
AFO (Gasienica-Jozkowsy et al., 2021)	Human Annotation	<b>18</b>	0.8%
Visdrone (Zhu et al., 2021)	Human Annotation	<b>416</b>	18.9%
Seadronesee (Varga et al., 2022)	Human Annotation	<b>3</b>	0.1%
ERA (Mou et al., in press)	Human Annotation	<b>363</b>	16.5%
CARLA (Dosovitskiy et al., 2017)	Simulation Script	<b>290</b>	13.2%
<b>Additional New Data Used In Case Study</b>			
CARLA (Dosovitskiy et al., 2017)	Simulation Script	<b>1500</b>	-
GTA V	Human Annotation	<b>400</b>	-

control over object instances (e.g., vehicles), supporting systematic evaluation of object counting performance (Section 3) and altitude-dependent detection studies (Section 5).

### 3.2.2 DATA IMPLEMENTATION

TDBench includes two task types: Multiple Choice Questions (MCQs) for most abilities, and Visual Grounding (VG). Each MCQ problem is structured as a quadruple  $P_i = [Q_i, I_i, C_i, L_i]$ , where  $Q_i$  denotes the textual question,  $I_i$  is the associated image,  $C_i$  represents the set of possible answers with  $n$  ( $2 \leq n \leq 4$ ) choices  $\{c_1, c_2, \dots, c_n\}$  (randomly shuffled during evaluation), and  $L_i$  is the correct label. For VG problems, we evaluate models’ ability to precisely localize objects by comparing their predicted bounding box coordinates against  $L_i$ , which contains human-annotated ground truth coordinates.

**Image Standardization** To mitigate evaluation biases from inconsistent image preprocessing across different VLMs (such as padding, stretching, or multi-tiling), we established a uniform input pipeline. All images were standardized to a fixed 512×512 pixel resolution. For tasks requiring image pairs, such as temporal or comparative analyses, we concatenated two sub-images either horizontally (as a 512×256 pair) or vertically (as a 256×512 pair). This method ensures the combined input fits the same 512×512 canvas, providing a fair and consistent basis for model comparison.

**Quality Control** We followed a two-stage quality control pipeline combining human and model-based checks. *Stage 1: Human review.* Six annotators independently examined all questions, removing or revising questions that were unsolvable due to lost context in the question, or that contained unclear wording or incorrect ground truth. *Stage 2: Model filtering.* Several open-source models (Deepseek VL2-small, InternVL2.5-MPO, Phi4, and Qwen2.5-VL 7B) were benchmarked to identify questions that were consistently failed or consistently solved across all models. Questions that all models failed underwent additional human review and were retained only if they were correctly formulated. Conversely, questions that all models solved were removed from TDBench since they offered little discriminative value for model comparison.

### 3.3 TDBENCH STATISTICS

TDBench contains 2000 problems across the 10 ability categories for each rotation, plus an additional 2100 problems used in four case studies. We aimed for an even distribution of problems across abilities, with 200 samples per category. Of the total questions, 1910 (including case studies) are collected from real-world datasets, and 2190 are generated from simulation environments. Notably, all problems in the ‘Object Counting’ category are generated from the CARLA Simulator, which allows controlled ground-truth labeling during scene generation. Under RotationalEval (RE), each question is evaluated across four orientations, effectively producing four instances per problem.

### 3.4 LEVERAGING ROTATIONAL INVARIANCE IN EVALUATION

In TDBench, we introduce a novel evaluation strategy, **RotationalEval (RE)**, designed to leverage the unique properties of top-down images (Figure 3, example from *object localization*). RE evaluates

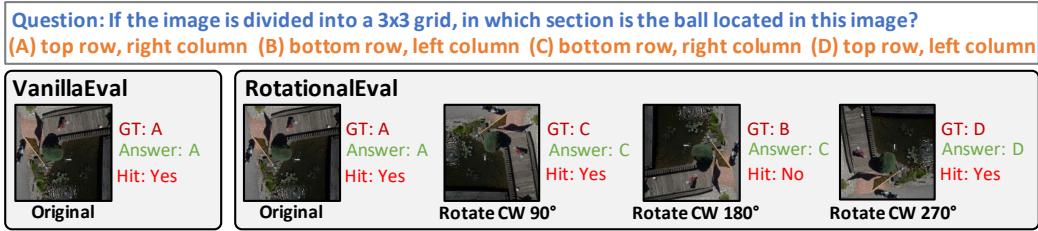


Figure 3: **Proposed RotationalEval (RE) strategy.** In RE, each image is rotated three times to create four questions, with choices generated separately for each rotation. We illustrate a failure case in *object localization* where four choices align with four images, and the VLM answers three correctly but fails on one.

model performance on four orientations of each image: the original, 90°, 180°, and 270° rotations, and counts a question as correct only if **all** four are answered correctly. This exploits the fundamental **rotational invariance** of aerial perspectives: unlike front-view images, where orientation conveys semantic information, top-down images preserve their meaning across rotations. Such rotations simply mimic different yaw angles during capture without altering scene content or physical spatial relationships. This property enables more rigorous evaluation, which would be unsuitable for front-view images where rotations create physically implausible scenes.

**Rotation-Aware Question Design** Because TDBench supports RotationalEval (RE), we categorized all questions as either **rotation-invariant** or **rotation-sensitive**. Rotation-invariant questions (e.g., object presence, attribute recognition) remain semantically unchanged after rotation; only the image is rotated while the question and answer options remain the same. Rotation-sensitive questions (e.g., spatial relationships or localization) require synchronized transformation of directional references. For instance, after a 90° clockwise rotation, phrases like “top-left” are mapped to “top-right”. To automate this process, we use placeholder tokens ( $\langle \text{img1} \rangle$ ,  $\langle \text{img2} \rangle$ ) in both questions and answers. In the original orientation, they are rendered as “left/right” or “top/bottom”, and these tokens are automatically rotated when generating the 90°, 180°, and 270° variants. This ensures consistent semantics across all rotation conditions.

## 4 EVALUATION RESULTS

### 4.1 SETUP

To ensure reproducibility and a fair comparison across models, all evaluations are conducted with VLMEvalKit (Duan et al., 2024), an open-source VLM evaluation framework. We evaluated a total of 60 VLMs in a zero-shot setting, without providing any in-context examples. For all experiments, the model temperature was set to 0, and GPT-4o was used as the answer extractor for all model outputs.

**Models** We evaluated 17 **proprietary models**, including the Claude (Anthropic, 2024; 2025a;c;b), Gemini (Google, 2024; 2025a), and GPT (OpenAI, 2024; 2025a;c;b) families; and 43 **open-source models** from diverse families such as Gemma 3 (Google, 2025b), InternVL (Chen et al., 2025; Zhu et al., 2025; Wang et al., 2025), Qwen2.5-VL (Bai et al., 2025a), DeepSeek VL2 (Wu et al., 2024), LLaVA (Liu et al., 2023; Li et al., 2024b), Kimi-VL (KimiTeam, 2025), and VLM-R1 (Shen et al., 2025). These models span a wide range of sizes, from 0.5 billion to 38 billion parameters.

### 4.2 RESULTS

**RotationalEval vs. VanillaEval** We first compare our proposed RotationalEval (RE) with the conventional one-pass evaluation, VanillaEval (VE). In this experiment, we use images without any rotations, denoted as  $\text{VE}@0^\circ$ . Table 2 summarizes their results on TDBench, averaged across all dimensions. Adopting RE leads to a notable performance decline across all VLMs. This drop occurs because RE reduces the chance of obtaining correct answers through random guessing. Interestingly, models with higher VE do not necessarily achieve higher RE. For example, although Gemini 1.5 Pro has a slightly lower VE than GPT-5 (0.756 vs. 0.761), it attains a higher RE (0.572 vs. 0.570). Among

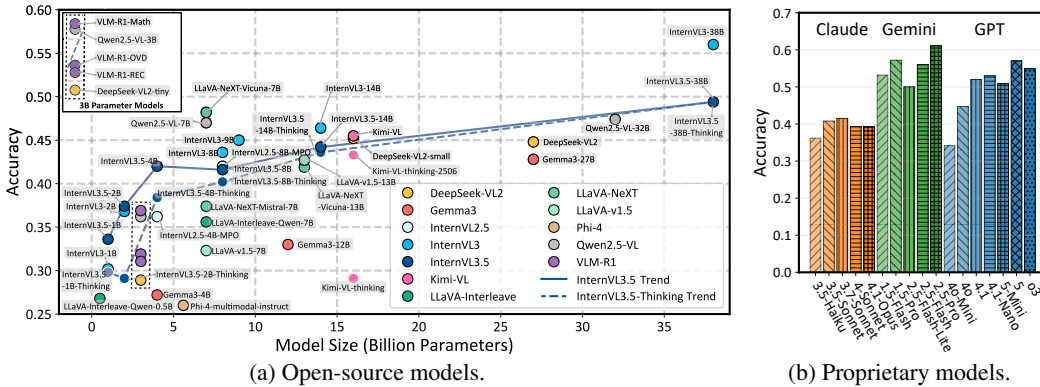


Figure 4: Average RE performance of models on TDBench, aggregated across 10 evaluation dimensions for both Open-source and Proprietary models.

open models, DeepSeek VL2 achieves the best VE, while Qwen2.5-VL-7B achieves the highest RE. These results suggest that models performing well under VE may still be prone to hallucinations, which we further examine in Section 4.3.

**Main Results** All reported results are based on **RotationalEval (RE)**, calculated as the *average* across ten evaluation categories unless explicitly stated. Detailed results, including *dimension-wise performance*, are provided in Appendix B.

Figure 4a shows the RE performance of various open-source models as a function of their parameter size. Within the same model families, performance generally increases with model size, although several exceptions exist. Notably, the “*thinking*” variants consistently underperform their standard counterparts, especially at smaller model sizes, with the gap narrowing as model size increases. This suggests that while chain-of-thought prompting can enhance reasoning at the semantic level, it may make responses less grounded in the visual input. In addition, newer models do not necessarily perform better: for example, InternVL3.5 underperforms InternVL3 despite being trained on more data, suggesting that additional general-purpose data may have diluted the proportion of top-down-related images during training. We also report the performance of proprietary models in Figure 4b; although their parameter sizes are undisclosed, the largest variants generally outperform their smaller counterparts, except for GPT-4.1 and GPT-4.1-Nano.

### 4.3 BEYOND ACCURACY: A DEEPER ANALYSIS OF MODEL RELIABILITY

As noted earlier, RotationalEval (RE) yields lower scores than VanillaEval (VE) because it discounts isolated correct predictions and thus reduces the impact of lucky guesses. To further analyze this phenomenon, let  $\Phi = \{0^\circ, 90^\circ, 180^\circ, 270^\circ\}$  be the set of rotations, and let  $Y_i^{(\phi)} \in \{0, 1\}$  denote whether the question  $i$  under rotation  $\phi$  is answered correctly. We define three observations

$$\text{RE} = \Pr(\forall \phi \in \Phi : Y_i^{(\phi)} = 1), \quad \overline{\text{VE}} = \mathbb{E}\left[\frac{1}{|\Phi|} \sum_{\phi \in \Phi} Y_i^{(\phi)}\right], \quad \text{MA} = \Pr(\forall \phi : Y_i^{(\phi)} = 0),$$

Table 2: Performance comparison of open-source and proprietary VLMs under VanillaEval (VE@0°) and RotationalEval (RE), along with the corresponding accuracy drop ( $\Delta$ ) on TDBench.

Open VLMs	VE	RE	$\Delta$	Prop VLMs	VE	RE	$\Delta$
Qwen2.5-VL 7B	0.630	<b>0.470</b>	<b>-0.160</b>	Gemini 2.5 Pro	<b>0.793</b>	<b>0.611</b>	<b>-0.182</b>
Kimi-VL	0.624	0.455	<b>-0.169</b>	Gemini 1.5 Pro	0.756	0.572	<b>-0.183</b>
DeepSeek VL2	<b>0.637</b>	0.448	<b>-0.189</b>	GPT-5	0.761	0.570	<b>-0.190</b>
InternVL3.5 14B	0.601	0.442	<b>-0.159</b>	GPT-4.1	0.720	0.520	<b>-0.200</b>
LLaVA-Next-13B	0.617	0.419	<b>-0.198</b>	Claude Sonnet 3.7	0.611	0.415	<b>-0.196</b>
Gemma3 12B	0.591	0.330	<b>-0.260</b>	Claude Opus 4.1	0.603	0.392	<b>-0.211</b>

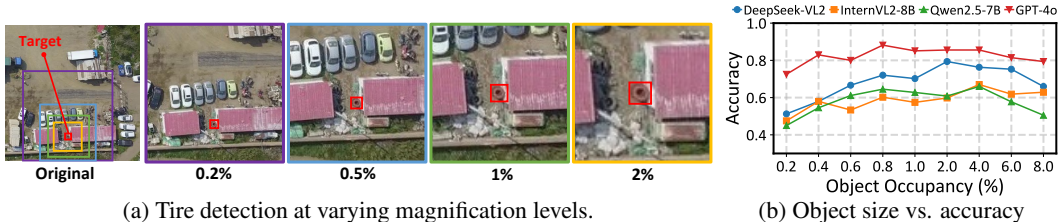


Figure 5: Impact of digital magnification on aerial object detection performance.

where MA denotes wrong answer in all rotations. Assuming each question for the model is either “known” or “unknown”, and rotations are conditionally independent, the above observations satisfy

$$\text{RE} = \theta r^4 + (1 - \theta)g^4, \quad \overline{\text{VE}} = \theta r + (1 - \theta)g, \quad \text{MA} = \theta(1 - r)^4 + (1 - \theta)(1 - g)^4.$$

where  $\theta$  represents the proportion of questions the model truly knows,  $r$  means the accuracy on known questions, and  $g$  denotes the accuracy on unknown questions (due to lucky guesses). These parameters are inferred by solving the system of equations above (see Appendix A for derivation); We aggregate these into the adjusted accuracy ( $A_{\text{adj}}$ ):

$$A_{\text{adj}} = \theta \cdot r.$$

The adjusted accuracy represents single-pass accuracy after discounting the contribution of guessing from the apparent correctness (VE). To illustrate this, Figure 1 (Right) presents results for different sizes of InternVL3, averaged across all evaluation dimensions. As model size increases,  $\theta$  (the proportion of questions the model truly knows) also rises, while  $r$  remains consistently high (approaching 100%), and shows a gradual upward trend with scale, which is desirable. In contrast,  $g$  exhibits variability that does not show a clear dependence on model size. Overall, Adjusted Accuracy improves with larger models, supporting the validity of our probability-based knowledge reliability analysis. Table 3 reports additional representative results across different model families (including four proprietary and four open-source VLMs), with full category-wise breakdowns for all 60 models provided in Appendix B.

Unlike the scaling trend observed with InternVL3, different models exhibit distinct strengths and weaknesses on TDBench. For example, *Gemini 2.5 Pro* achieves the highest  $\theta$ , suggesting it possesses the broadest knowledge coverage, although its  $r$  is lower than that of OpenAI’s GPT-5 and o3. Both GPT-5 and o3, however, yield the highest  $g$  values, indicating that these models are more likely to produce correct answers by chance. On the other hand, *Gemma3-27B* shows the lowest  $\theta$ , indicating a comparatively narrower knowledge base. Meanwhile, *Claude Opus 4.1* shows the lowest  $r$  among all models, even below all open-source models listed here, which may stem from its stronger emphasis on code-related reasoning or function-calling tasks rather than visual–language understanding.

Table 3: RE, MA,  $\overline{\text{VE}}$ , and reliability parameters (proportion of questions a model truly knows  $\theta$ , accuracy among known questions  $r$ , accuracy among guessed questions  $g$ , and adjusted accuracy  $A_{\text{adj}}$ ). Arrows indicate whether higher ( $\uparrow$ ) or lower ( $\downarrow$ ) is better. Best values are green, worst are red.

Model	RE $\uparrow$	MA $\downarrow$	$\overline{\text{VE}}\uparrow$	$\theta\uparrow$	$r\uparrow$	$g$	$A_{\text{adj}}\uparrow$
Gemini 2.5 Pro	<b>0.611</b>	<b>0.073</b>	<b>0.791</b>	<b>0.822</b>	0.909	0.201	<b>0.754</b>
GPT-5	0.570	0.085	0.751	0.688	<b>0.941</b>	0.265	0.652
Claude Opus 4.1	<b>0.392</b>	0.194	0.607	0.610	<b>0.849</b>	0.189	0.541
o3	0.549	0.096	0.731	0.693	0.921	0.279	0.651
DeepSeek VL2	0.448	0.196	0.631	0.620	0.900	0.184	0.568
Gemma3-27B	0.428	0.220	<b>0.604</b>	<b>0.587</b>	0.880	0.206	<b>0.538</b>
Qwen2.5-VL-32B	0.474	0.165	0.668	0.668	0.902	0.203	0.611
Kimi-VL	0.455	<b>0.239</b>	0.613	0.612	0.882	0.164	0.565

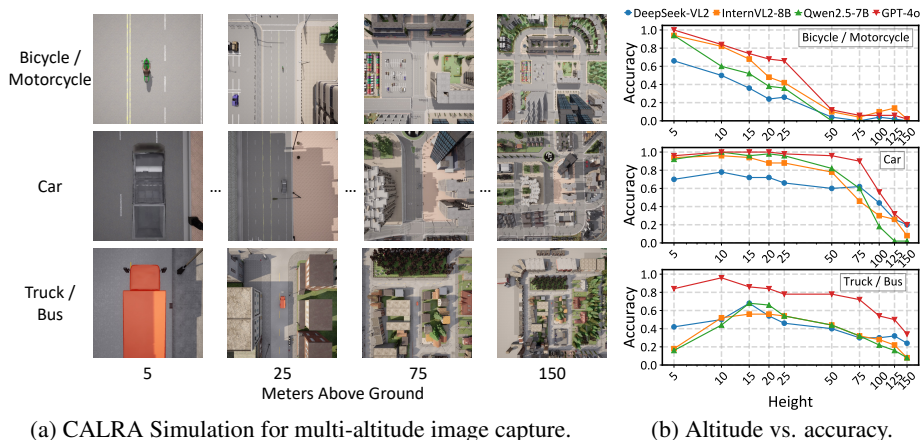


Figure 6: Impact of camera altitude on object detection performance. The right plot shows detection accuracy as a function of altitude (5-150m) on a logarithmic scale.



Figure 7: Example of Integrity study. (a) Three different area ratios (AR) ( $25\times$ ,  $50\times$ ,  $100\times$ ). (b), (c), and (d) show visibility ratios of 30%, 60%, and 90%, respectively, in the setting ( $AR=25\times$ ), depending on how much of the object is bounded inside the image cropped regions.

## 5 CASE STUDIES

Top-down images are typically captured from high altitudes, which introduces unique challenges such as small object size, unusual perspective, and the lack of depth cues, yet depth is critical for tasks like building height estimation or drone navigation. To examine these challenges, we design four targeted case studies.

### 5.1 CASE STUDY 1: DIGITAL MAGNIFICATION FOR SMALL OBJECT DETECTION

Small objects occupy very few pixels, making them difficult for VLMs to detect. We explore a *digital magnification* strategy that crops images to increase the target object’s relative pixel coverage (area ratio), as illustrated in Figure 5a. We use samples from *object presence* and *object localization* tasks where baseline performance was low, and reformat them using the *object presence* template.

Figure 5b shows that accuracy rises with area ratio before dropping as context is lost. GPT-4o peaks at only 0.8% occupancy, whereas open-source models require 2–4%. Beyond 6%, performance declines across all models due to resolution loss and reduced context. These findings offer practical guidance on magnification levels for aerial imaging and suggest future work on improving small-object detection in VLMs, particularly for models using multi-tile preprocessing, where tile size could be adapted based on prior knowledge of target object scale.

### 5.2 CASE STUDY 2: ALTITUDE EFFECTS ON OBJECT DETECTION

This study examines optimal hovering heights for drones with a fixed field of view (FOV) when performing tasks that require consistent object detection, such as tracking suspects. Unlike previous studies, we focus on physical “zoom-in”, where the drone adjusts its altitude to improve detection performance. Because most datasets lack camera height metadata, we used the CARLA simulation to deploy multiple cameras at different altitudes over identical scenes (Figure 6a). We evaluated three

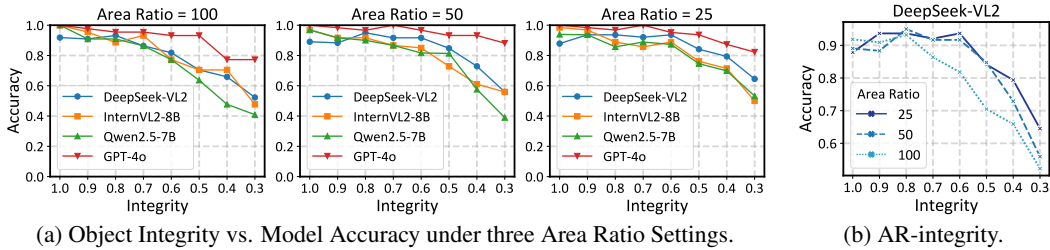


Figure 8: Impact of Object Integrity and Area Ratio on VLM Performance.

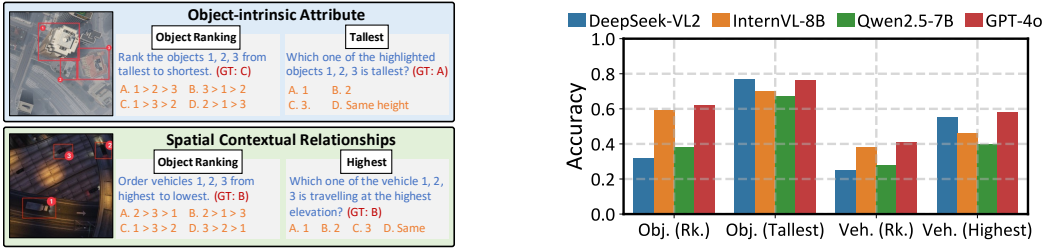


Figure 9: Analysis of spatial awareness and depth perception.

object categories (bicycle/motorcycle, car, and truck/bus)—chosen for their frequency in aerial tasks and distinct size differences. *Object presence performance* was measured across altitudes from 5 to 150 meters, spanning typical operational ranges for commercial and tactical drones, while keeping image resolution constant. This setup offers practical guidance for maximizing detection reliability through optimal drone positioning rather than post-capture image processing.

As shown in Figure 6b, accuracy generally decreases with altitude but peaks at specific heights: 5m for bicycles/motorcycles, 10m for cars, and 15m for trucks/buses. We attribute this to field coverage differences: at low altitudes, large objects may be only partially visible, reducing detection accuracy, while smaller objects remain fully visible even at minimal heights.

### 5.3 CASE STUDY 3: OBJECT VISIBILITY AND PARTIAL OCCLUSION

Objects may be only partially visible, especially near image borders. We controlled visibility (**integrity**) by shifting a fixed-size crop window over objects at a set area ratio (AR) (Figure 7). This allowed us to vary integrity while keeping magnification constant.

Figure 8a shows that accuracy stays stable ( $\geq 90\%$ ) until integrity drops below a threshold, then declines sharply. This threshold depends on AR: with AR=100, accuracy drops below 70% integrity, while lower ARs fail around 60% (Figure 8b). This demonstrates how incomplete visibility affects detection even without resolution changes.

### 5.4 CASE STUDY 4: Z-AXIS PERCEPTION AND DEPTH UNDERSTANDING

Since top-down images preserve xy-plane information, they inherently lack altitude cues. To evaluate this limitation, we defined two types of **z-axis awareness** challenges (Figure 9a): (i) assessing an object’s intrinsic properties, such as a building’s or tree’s height, and (ii) evaluating contextual relationships, such as determining whether a car is traveling on a road or an overpass. As shown in Figure 9b, DeepSeek performs well on tallest/highest identification but struggles with ranking tasks, whereas GPT-4o achieves near-best performance across both types.

## 6 DISCUSSION

**Probing Intrinsic Model Properties** Although we introduce these metrics within the context of TDBench, they should not be viewed as entirely independent of the dataset. Rather, TDBench provides a controlled medium to probe latent aspects of model behavior that are difficult to observe

---

otherwise. The estimated parameters  $(\theta, r, g)$  offer a useful abstraction of how much correctness stems from genuine knowledge versus chance, but their validity ultimately depends on the diversity and fidelity of the underlying data. Future work should compare these estimates across multiple datasets and domains to confirm whether they generalize as truly model-intrinsic properties.

**Difference with Multi-Pass Evaluation and Majority Voting** Unlike multi-pass evaluation with majority voting, which explores variability in stochastic decoding, our RotationalEval (RE) assesses invariance under controlled changes to the visual input. This makes RE more diagnostic of grounding and invariance. At the same time, RE introduces stricter success criteria, which may amplify penalties for minor inconsistencies or ambiguous visual cases. Thus, we view RE as complementary to multi-pass evaluation: the former highlights robustness to perceptual transformations, while the latter captures robustness to sampling variance.

**Limitations of TDBench** Our work has several limitations. (1) The current benchmark includes 2,000 core questions and additional case-study questions, which, although carefully curated, remain relatively small compared to large-scale multimodal datasets. We are working to expand both the size and diversity of the benchmark. (2) Except for visual grounding tasks, correctness of generated responses is determined by an extractor model, and our reported results rely on GPT-4o. This introduces possible bias and raises the need for extractor-agnostic evaluation. (3) A significant portion of case studies in the benchmark is based on simulation, which allows precise control but may not fully capture the variability of real-world aerial images. Future iterations should incorporate larger amounts of real data.

## 7 CONCLUSION

In this work, we introduced TDBench, a comprehensive benchmark for evaluating VLMs on top-down images, comprising over 2,000 manually labeled questions across diverse categories. To ensure robust and reliable assessment, we proposed **RotationalEval**, an evaluation strategy that leverages the rotational invariance of top-down perspectives to provide a more rigorous alternative to standard single-pass evaluation. Beyond accuracy, we further developed a set of **reliability-oriented metrics** that assess how much of a model’s performance stems from genuine knowledge rather than lucky guesses or hallucinated responses. Our multi-dimensional analysis reveals both the capabilities and limitations of current VLMs, and our four case studies demonstrate their strengths and challenges in real-world aerial applications. While TDBench serves as the testbed for this study, these metrics are not tied to any specific dataset and can serve as **general probes of model reliability**, offering a new perspective for guiding future development of more trustworthy VLMs.

## REFERENCES

- Anthropic. Claude 3.5 sonnet, 2024. URL <https://www.anthropic.com/news/claude-3-5-sonnet>. Accessed: 2025-03-26.
- Anthropic. Claude 3.7 sonnet, 2025a. URL <https://www.anthropic.com/news/claude-3-7-sonnet>. Accessed: 2025-09-16.
- Anthropic. Claude 4.1, 2025b. URL <https://www.anthropic.com/news/claude-opus-4-1>. Accessed: 2025-09-16.
- Anthropic. Claude 4, 2025c. URL <https://www.anthropic.com/news/claude-4>. Accessed: 2025-09-16.
- Shuai Bai, Keqin Chen, and Xuejing Liu et al. Qwen2.5-vl technical report. *arXiv preprint arXiv:2502.13923*, 2025a.
- Zechen Bai, Pichao Wang, Tianjun Xiao, Tong He, Zongbo Han, Zheng Zhang, and Mike Zheng Shou. Hallucination of multimodal large language models: A survey, 2025b. URL <https://arxiv.org/abs/2404.18930>.

- 
- Zhe Chen, Weiyun Wang, Yue Cao, Yangzhou Liu, Zhangwei Gao, et al. Expanding performance boundaries of open-source multimodal models with model, data, and test-time scaling, 2025. URL <https://arxiv.org/abs/2412.05271>.
- Muhammad Sohail Danish, Muhammad Akhtar Munir, Syed Roshaan Ali Shah, Kartik Kuckreja, Fahad Shahbaz Khan, Paolo Fraccaro, Alexandre Lacoste, and Salman Khan. Geobench-vlm: Benchmarking vision-language models for geospatial tasks, 2025. URL <https://arxiv.org/abs/2411.19325>.
- Alexey Dosovitskiy, German Ros, Felipe Codevilla, Antonio Lopez, and Vladlen Koltun. CARLA: An open urban driving simulator. In *Proceedings of the 1st Annual Conference on Robot Learning*, pp. 1–16, 2017.
- Haodong Duan, Junming Yang, Yuxuan Qiao, Xinyu Fang, Lin Chen, Yuan Liu, Xiaoyi Dong, Yuhang Zang, Pan Zhang, Jiaqi Wang, et al. Vlmevalkit: An open-source toolkit for evaluating large multi-modality models. In *Proceedings of the 32nd ACM International Conference on Multimedia*, pp. 11198–11201, 2024.
- Chaoyou Fu, Peixian Chen, Yunhang Shen, Yulei Qin, Mengdan Zhang, Xu Lin, Jinrui Yang, Xiawu Zheng, Ke Li, Xing Sun, Yunsheng Wu, and Rongrong Ji. Mme: A comprehensive evaluation benchmark for multimodal large language models, 2024. URL <https://arxiv.org/abs/2306.13394>.
- Jan Gasienica-Jozkowsy, Mateusz Knapik, and Boguslaw Cyganek. An ensemble deep learning method with optimized weights for drone-based water rescue and surveillance. *Integrated Computer-Aided Engineering*, 28(1):1–15, 01 2021. doi: 10.3233/ICA-210649.
- Google. Gemini 1.5: Unlocking multimodal understanding across millions of tokens of context, 2024. URL <https://arxiv.org/abs/2403.05530>.
- Google. Gemini 2.5: Pushing the frontier with advanced reasoning, multimodality, long context, and next generation agentic capabilities, 2025a. URL <https://arxiv.org/abs/2507.06261>.
- Google. Gemma 3 technical report, 2025b. URL <https://arxiv.org/abs/2503.19786>.
- Tianrui Guan, Fuxiao Liu, Xiyang Wu, Ruiqi Xian, Zongxia Li, Xiaoyu Liu, Xijun Wang, Lichang Chen, Furong Huang, Yaser Yacoob, Dinesh Manocha, and Tianyi Zhou. Hallusionbench: An advanced diagnostic suite for entangled language hallucination and visual illusion in large vision-language models, 2024. URL <https://arxiv.org/abs/2310.14566>.
- Yuan Hu, Jianlong Yuan, Congcong Wen, Xiaonan Lu, and Xiang Li. Rsgpt: A remote sensing vision language model and benchmark, 2023. URL <https://arxiv.org/abs/2307.15266>.
- ICG. Semantic segmentation drone dataset, 2019. URL <http://dronedataset.icg.tugraz.at/>.
- KimiTeam. Kimi-vl technical report, 2025. URL <https://arxiv.org/abs/2504.07491>.
- Kartik Kuckreja, Muhammad Sohail Danish, Muzammal Naseer, Abhijit Das, Salman Khan, and Fahad Shahbaz Khan. Geochat: Grounded large vision-language model for remote sensing, 2023. URL <https://arxiv.org/abs/2311.15826>.
- Chengzu Li, Caiqi Zhang, Han Zhou, Nigel Collier, Anna Korhonen, and Ivan Vulić. Topviews: Vision-language models as top-view spatial reasoners, 2024a. URL <https://arxiv.org/abs/2406.02537>.
- Feng Li, Renrui Zhang, Hao Zhang, Yuanhan Zhang, Bo Li, Wei Li, Zejun Ma, and Chunyuan Li. Llava-next-interleave: Tackling multi-image, video, and 3d in large multimodal models. *arXiv preprint arXiv:2407.07895*, 2024b.
- Yifan Li, Yifan Du, Kun Zhou, Jinpeng Wang, Wayne Xin Zhao, and Ji-Rong Wen. Evaluating object hallucination in large vision-language models, 2023a. URL <https://arxiv.org/abs/2305.10355>.

- 
- Yifan Li, Yifan Du, Kun Zhou, Jinpeng Wang, Xin Zhao, and Ji-Rong Wen. Evaluating object hallucination in large vision-language models. In Houda Bouamor, Juan Pino, and Kalika Bali (eds.), *Proceedings of the 2023 Conference on Empirical Methods in Natural Language Processing*, pp. 292–305, Singapore, December 2023b. Association for Computational Linguistics. doi: 10.18653/v1/2023.emnlp-main.20. URL <https://aclanthology.org/2023.emnlp-main.20/>.
- Tsung-Yi Lin, Michael Maire, Serge Belongie, Lubomir Bourdev, Ross Girshick, James Hays, Pietro Perona, Deva Ramanan, C. Lawrence Zitnick, and Piotr Dollár. Microsoft coco: Common objects in context, 2015. URL <https://arxiv.org/abs/1405.0312>.
- Hanchao Liu, Wenyuan Xue, Yifei Chen, Dapeng Chen, Xiutian Zhao, Ke Wang, Liping Hou, Rongjun Li, and Wei Peng. A survey on hallucination in large vision-language models, 2024a. URL <https://arxiv.org/abs/2402.00253>.
- Haotian Liu, Chunyuan Li, Qingyang Wu, and Yong Jae Lee. Visual instruction tuning. In *NeurIPS*, 2023.
- Yuan Liu, Haodong Duan, Yuanhan Zhang, Bo Li, Songyang Zhang, Wangbo Zhao, Yike Yuan, Jiaqi Wang, Conghui He, Ziwei Liu, Kai Chen, and Dahua Lin. Mmbench: Is your multi-modal model an all-around player?, 2024b. URL <https://arxiv.org/abs/2307.06281>.
- Pan Lu, Hritik Bansal, Tony Xia, Jiacheng Liu, Chunyuan Li, Hannaneh Hajishirzi, Hao Cheng, Kai-Wei Chang, Michel Galley, and Jianfeng Gao. Mathvista: Evaluating mathematical reasoning of foundation models in visual contexts, 2024. URL <https://arxiv.org/abs/2310.02255>.
- Yuncheng Lu, Zhucun Xue, Gui-Song Xia, and Liangpei Zhang. A survey on vision-based uav navigation. *Geo-spatial Information Science*, 21(1):21–32, 2018. doi: 10.1080/10095020.2017.1420509. URL <https://doi.org/10.1080/10095020.2017.1420509>.
- L. Mou, Y. Hua, P. Jin, and X. X. Zhu. ERA: A dataset and deep learning benchmark for event recognition in aerial videos. *IEEE Geoscience and Remote Sensing Magazine*, in press.
- Dilxat Muhtar, Zhenshi Li, Feng Gu, Xueliang Zhang, and Pengfeng Xiao. Lhrs-bot: Empowering remote sensing with vgi-enhanced large multimodal language model, 2024. URL <https://arxiv.org/abs/2402.02544>.
- Nearmap. How aerial imagery revolutionizes urban planning, 2022. URL <https://www.nearmap.com/blog/how-aerial-imagery-revolutionizes-urban-planning>. Accessed: 2025-09-16.
- OpenAI. Gpt-4 technical report, 2024. URL <https://arxiv.org/abs/2303.08774>.
- OpenAI. Introducing gpt-4.1 in the api, 2025a. URL <https://openai.com/index/gpt-4-1/>. Accessed: 2025-09-16.
- OpenAI. Introducing gpt-5, 2025b. URL <https://openai.com/index/introducing-gpt-5/>. Accessed: 2025-09-16.
- OpenAI. Introducing openai o3 and o4-mini, 2025c. URL <https://openai.com/index/introducing-o3-and-o4-mini/>. Accessed: 2025-09-16.
- Alec Radford, Jong Wook Kim, Chris Hallacy, Aditya Ramesh, Gabriel Goh, Sandhini Agarwal, Girish Sastry, Amanda Askell, Pamela Mishkin, Jack Clark, Gretchen Krueger, and Ilya Sutskever. Learning transferable visual models from natural language supervision, 2021. URL <https://arxiv.org/abs/2103.00020>.
- Olga Russakovsky, Jia Deng, Hao Su, Jonathan Krause, Sanjeev Satheesh, Sean Ma, Zhiheng Huang, Andrej Karpathy, Aditya Khosla, Michael Bernstein, Alexander C. Berg, and Li Fei-Fei. Imagenet large scale visual recognition challenge, 2015. URL <https://arxiv.org/abs/1409.0575>.

- 
- Christoph Schuhmann, Romain Beaumont, Richard Vencu, Cade Gordon, Ross Wightman, Mehdi Cherti, Theo Coombes, Aarush Katta, Clayton Mullis, Mitchell Wortsman, Patrick Schramowski, Srivatsa Kundurthy, Katherine Crowson, Ludwig Schmidt, Robert Kaczmarczyk, and Jenia Jitsev. Laion-5b: An open large-scale dataset for training next generation image-text models, 2022. URL <https://arxiv.org/abs/2210.08402>.
- Shaha. Aerial traffic images. <https://universe.roboflow.com/cg-0fmsf/shaha-ady7>, 2025. Accessed: 2025-03-26.
- Haozhan Shen, Peng Liu, Jingcheng Li, Chunxin Fang, Yibo Ma, Jiajia Liao, Qiaoli Shen, Zilun Zhang, Kangjia Zhao, Qianqian Zhang, Ruochen Xu, and Tiancheng Zhao. Vlm-r1: A stable and generalizable r1-style large vision-language model, 2025. URL <https://arxiv.org/abs/2504.07615>.
- Leon Amadeus Varga, Benjamin Kiefer, Martin Messmer, and Andreas Zell. Seadronessee: A maritime benchmark for detecting humans in open water. In *Proceedings of the IEEE/CVF Winter Conference on Applications of Computer Vision*, pp. 2260–2270, 2022.
- Chenxi Wang, Xiang Chen, Ningyu Zhang, Bozhong Tian, Haoming Xu, Shumin Deng, and Huajun Chen. Mlm can see? dynamic correction decoding for hallucination mitigation, 2024. URL <https://arxiv.org/abs/2410.11779>.
- Weiyun Wang, Zhangwei Gao, Lixin Gu, Hengjun Pu, et al. Internvl3.5: Advancing open-source multimodal models in versatility, reasoning, and efficiency, 2025. URL <https://arxiv.org/abs/2508.18265>.
- Zhiyu Wu, Xiaokang Chen, Zizheng Pan, et al. Deepseek-vl2: Mixture-of-experts vision-language models for advanced multimodal understanding, 2024. URL <https://arxiv.org/abs/2412.10302>.
- Weihao Yu, Zhengyuan Yang, Linjie Li, Jianfeng Wang, Kevin Lin, Zicheng Liu, Xinchao Wang, and Lijuan Wang. Mm-vet: Evaluating large multimodal models for integrated capabilities, 2024. URL <https://arxiv.org/abs/2308.02490>.
- Xiang Yue, Yuansheng Ni, Kai Zhang, Tianyu Zheng, Ruoqi Liu, Ge Zhang, Samuel Stevens, Dongfu Jiang, Weiming Ren, Yuxuan Sun, Cong Wei, Botao Yu, Ruibin Yuan, Renliang Sun, Ming Yin, Boyuan Zheng, Zhenzhu Yang, Yibo Liu, Wenhao Huang, Huan Sun, Yu Su, and Wenhua Chen. Mmmu: A massive multi-discipline multimodal understanding and reasoning benchmark for expert agi, 2024. URL <https://arxiv.org/abs/2311.16502>.
- Xiaohua Zhai, Basil Mustafa, Alexander Kolesnikov, and Lucas Beyer. Sigmoid loss for language image pre-training, 2023. URL <https://arxiv.org/abs/2303.15343>.
- Minghui Zhao, Junxi Xia, Kaiyuan Hou, Yanchen Liu, Stephen Xia, and Xiaofan Jiang. *FlexiFly: Interfacing the Physical World with Foundation Models Empowered by Reconfigurable Drone Systems*, pp. 463–476. Association for Computing Machinery, New York, NY, USA, 2025. ISBN 9798400714795. URL <https://doi.org/10.1145/3715014.3722081>.
- Jinguo Zhu, Weiyun Wang, Zhe Chen, Zhaoyang Liu, Shenglong Ye, et al. Internvl3: Exploring advanced training and test-time recipes for open-source multimodal models, 2025. URL <https://arxiv.org/abs/2504.10479>.
- Pengfei Zhu, Longyin Wen, Dawei Du, Xiao Bian, Heng Fan, Qinghua Hu, and Haibin Ling. Detection and tracking meet drones challenge. *IEEE Transactions on Pattern Analysis and Machine Intelligence*, 44(11):7380–7399, 2021.

# Appendix

## A IDENTIFIABILITY OF THE MIXTURE PARAMETERS

We used three parameters,  $(\theta, r, g) \in [0, 1]^3$  to study the reliability of the models. These parameters denote the proportion of questions a model truly knows ( $\theta$ ), model's accuracy among the questions that it knows ( $r$ ), and model's accuracy among the questions it does not know and guessed ( $g$ ).

We show that these parameters in our mixture model are *generically unique* given the observed statistics

$$\text{RE}, \quad \overline{\text{VE}}, \quad \text{MA}.$$

### A.1 PROBLEM FORMULATION

Assume the parameters satisfy

$$\begin{aligned} \text{RE} &= \theta r^4 + (1 - \theta)g^4, \\ \overline{\text{VE}} &= \theta r + (1 - \theta)g, \\ \text{MA} &= \theta(1 - r)^4 + (1 - \theta)(1 - g)^4. \end{aligned} \tag{1}$$

This system is symmetric under the transformation

$$(\theta, r, g) \longleftrightarrow (1 - \theta, g, r).$$

To remove this trivial multiplicity, we restrict to the *ordered domain*

$$\mathcal{D}_{\overline{\text{VE}}} := \{(r, g) \mid 0 \leq g < \overline{\text{VE}} < r \leq 1\}, \quad \theta = \frac{\overline{\text{VE}} - g}{r - g} \in (0, 1). \tag{2}$$

The degenerate case  $r = g$  occurs iff  $\text{RE} = \overline{\text{VE}}^4$  and  $\text{MA} = (1 - \overline{\text{VE}})^4$  and is excluded. We also exclude trivial boundary cases  $\overline{\text{VE}} \in \{0, 1\}$  or  $\text{MA} \in \{0, 1\}$ , where conditioning becomes ill-defined.

### A.2 REDUCTION TO SECANT EQUATIONS

Define  $f(x) = x^4$  and  $u(x) = (1 - x)^4$ . Eliminating  $\theta$  using the middle equation in equation 1, the outer equations become the *secant identities*

$$\boxed{\frac{\text{RE} - g^4}{\overline{\text{VE}} - g} = \frac{r^4 - g^4}{r - g}, \quad \frac{\text{MA} - (1 - g)^4}{\overline{\text{VE}} - g} = \frac{(1 - r)^4 - (1 - g)^4}{r - g}}. \tag{3}$$

These state that  $(g, r)$  have the same secant slope on  $f$  as  $(1 - g, 1 - r)$  do on  $u$ .

Since  $f$  and  $u$  are strictly convex on  $[0, 1]$ , their secant slopes are strictly increasing in each endpoint. In particular, for fixed  $g \in [0, 1]$ ,

$$r \mapsto \frac{r^4 - g^4}{r - g} \text{ is strictly increasing on } (g, 1]. \tag{4}$$

### A.3 ELIMINATION TO ONE VARIABLE

Using  $r^4 - g^4 = (r - g)(r^3 + gr^2 + g^2r + g^3)$ , the first equation in equation 3 is equivalent (for  $r \neq g$ ) to the cubic

$$r^3 + gr^2 + g^2r + g^3 = \frac{\text{RE} - g^4}{\overline{\text{VE}} - g}. \tag{5}$$

By equation 4, this has at most one solution  $r > g$  for each fixed  $g$ .

Let  $r = R(g)$  denote this unique solution (if it exists) and define

$$E(g) := \frac{(1 - R(g))^4 - (1 - g)^4}{R(g) - g} - \frac{\text{MA} - (1 - g)^4}{\overline{\text{VE}} - g}. \tag{6}$$

**Lemma (Bijection with  $E(g) = 0$ ).** For fixed  $\overline{\text{VE}} \in (0, 1)$ , ordered solutions  $(r, g) \in \mathcal{D}_{\overline{\text{VE}}}$  of equation 3 are in one-to-one correspondence with real roots  $g \in (0, \overline{\text{VE}})$  of  $E(g) = 0$  for which  $R(g) > \overline{\text{VE}}$ . For each such root  $g^*$ , the corresponding  $r^* = R(g^*)$  is unique, and then  $\theta^* = \frac{\overline{\text{VE}} - g^*}{r^* - g^*}$ .

**Proof.** Fix  $g \in (0, \overline{\text{VE}})$ . The first equality in equation 3 uniquely determines  $r = R(g) > g$  by equation 5; substituting into the second gives  $E(g) = 0$ . Conversely, if  $E(g) = 0$  and  $R(g) > \overline{\text{VE}}$ , then  $(\theta, r, g) = (\frac{\overline{\text{VE}} - g}{R(g) - g}, R(g), g)$  solves equation 1.  $\square$

**Remark (Why  $R(g) > \overline{\text{VE}}$ ).** Since  $x \mapsto x^4$  is convex on  $[0, 1]$ , Jensen's inequality gives  $\text{RE} = \theta r^4 + (1 - \theta)g^4 \geq (\theta r + (1 - \theta)g)^4 = \overline{\text{VE}}^4$ , with strict inequality in the ordered, nondegenerate case  $r \neq g$ . Hence

$$\frac{\text{RE} - g^4}{\overline{\text{VE}} - g} > \frac{\overline{\text{VE}}^4 - g^4}{\overline{\text{VE}} - g}.$$

By strict monotonicity in equation 4, the unique  $r$  satisfying the first secant identity must satisfy  $r = R(g) > \overline{\text{VE}}$ .

#### A.4 THE CUBIC IN $g$ AND ITS DISCRIMINANT

Clearing denominators in equation 3 yields a cubic polynomial

$$P_{\text{RE}, \overline{\text{VE}}, \text{MA}}(g) = 0, \tag{7}$$

whose coefficients depend algebraically on  $(\text{RE}, \overline{\text{VE}}, \text{MA})$ . *Degree justification.* Using equation 5, the first secant identity expresses  $\frac{r^4 - g^4}{r - g}$  as  $r^3 + gr^2 + g^2r + g^3$ , which is linear in the unknown slope  $\frac{\text{RE} - g^4}{\overline{\text{VE}} - g}$ ; substituting this  $r = R(g)$  into the second identity and clearing denominators cancels the factor  $(r - g)$  and leaves a polynomial of degree at most 3 in  $g$ . (Explicit coefficients are lengthy and omitted for brevity.)

By the lemma above, *ordered solutions* are in bijection with *real roots* of  $P_{\text{RE}, \overline{\text{VE}}, \text{MA}}(g)$  in  $(0, \overline{\text{VE}})$ .

Let  $\Delta(P)$  denote the discriminant of a cubic  $P(g) = ag^3 + bg^2 + cg + d$ :

$$\Delta(P) = 18abcd - 4b^3d + b^2c^2 - 4ac^3 - 27a^2d^2.$$

This determines the real root structure:

$$\Delta < 0 \Rightarrow \text{one real root}, \quad \Delta > 0 \Rightarrow \text{three real roots}, \quad \Delta = 0 \Rightarrow \text{a multiple real root}.$$

**Theorem (Uniqueness certificate).** Fix  $\overline{\text{VE}} \in (0, 1)$  and  $(\text{RE}, \text{MA})$ . Let  $P_{\text{RE}, \overline{\text{VE}}, \text{MA}}$  be as in equation 7. If  $\Delta(P_{\text{RE}, \overline{\text{VE}}, \text{MA}}) < 0$ , then there is at most one ordered solution  $(r, g) \in \mathcal{D}_{\overline{\text{VE}}}$ . If, in addition,  $P_{\text{RE}, \overline{\text{VE}}, \text{MA}}$  has a real root  $g^* \in (0, \overline{\text{VE}})$ , then

$$r^* = R(g^*), \quad \theta^* = \frac{\overline{\text{VE}} - g^*}{r^* - g^*}$$

gives the unique solution  $(\theta^*, r^*, g^*)$  of equation 1 up to symmetry.

**Proof.** Ordered solutions correspond to real roots of  $P_{\text{RE}, \overline{\text{VE}}, \text{MA}}(g)$  in  $(0, \overline{\text{VE}})$ . If  $\Delta < 0$  then  $P$  has a single real root on  $\mathbb{R}$ , hence at most one in  $(0, \overline{\text{VE}})$ . If such a root exists, the corresponding  $(r, g)$  and  $\theta$  are uniquely recovered via  $R(g)$  and equation 2.  $\square$

#### A.5 GENERIC UNIQUENESS AND THE DISCRIMINANT LOCUS

Let  $\mathcal{R}_{\overline{\text{VE}}}$  be the image of  $\mathcal{D}_{\overline{\text{VE}}}$  under the map  $(r, g) \mapsto (\text{RE}, \text{MA})$  defined by equation 3. The equation  $\Delta(P_{\text{RE}, \overline{\text{VE}}, \text{MA}}) = 0$  defines a real algebraic curve  $\Sigma_{\overline{\text{VE}}} \subset \mathcal{R}_{\overline{\text{VE}}}$  (the *discriminant locus*).

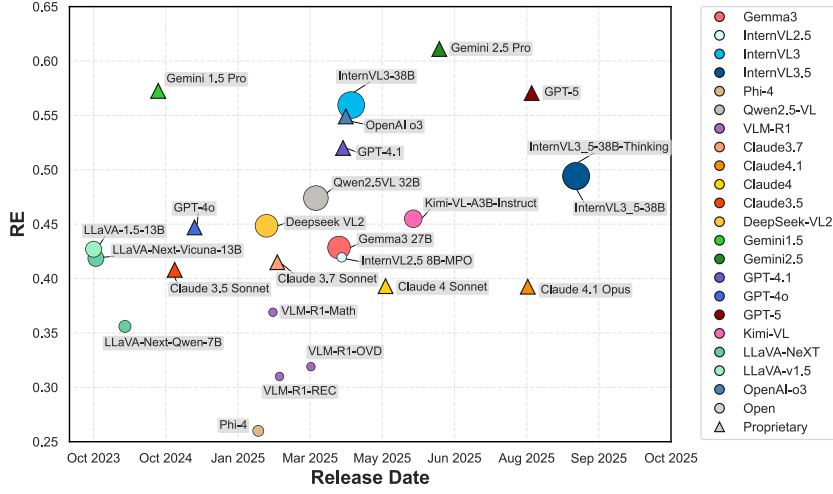


Figure 10: Performance (RE) of models versus their release date. Circles denote open-source models, with marker size indicating model scale. Triangles denote proprietary models. Each point represents the largest evaluated model from a given family.

**Theorem (Generic uniqueness).** For fixed  $\overline{VE} \in (0, 1)$ :

- If  $(RE, MA) \in \mathcal{R}_{\overline{VE}} \setminus \Sigma_{\overline{VE}}$ , then  $\Delta < 0$  and equation 1 has a unique solution  $(\theta, r, g)$  up to symmetry.
- If  $(RE, MA) \in \Sigma_{\overline{VE}}$ , then either a multiple solution occurs or three distinct solutions exist.

In particular,  $\Sigma_{\overline{VE}}$  has measure zero, so for almost all valid  $(RE, \overline{VE}, MA)$  the parameters  $(\theta, r, g)$  are uniquely identifiable up to symmetry.

**Proof (sketch).** Off  $\Sigma_{\overline{VE}}$  the simple-root condition  $(\partial P / \partial g) \neq 0$  holds generically; by continuity (implicit function theorem), the number of real roots is locally constant and equals 1, yielding a single ordered solution. On  $\Sigma_{\overline{VE}}$  the discriminant changes sign, creating a multiple or triple real root.  $\square$

**Existence note.** For statistics induced by any nondegenerate mixture in the ordered domain ( $r > \overline{VE} > g$ ), continuity of the forward map  $(r, g) \mapsto (RE, MA)$  and the intermediate value principle ensure that  $P_{RE, \overline{VE}, MA}(g)$  attains a real root in  $(0, \overline{VE})$ . Empirically, all rows in our dataset satisfy this condition.

## A.6 SUMMARY

The system equation 1 admits at most three ordered solutions (six with symmetry). However, generically  $\Delta < 0$ , so there is exactly one ordered solution (and thus one  $(\theta, r, g)$  up to symmetry). Empirically, our dataset lies in this generic region, which explains why the solver returns either zero or one solution per row.

## B ADDITIONAL EVALUATION RESULTS

### B.1 MODEL SCALING TRENDS

We further analyze model performance trends over time and model size. Figure 4a shows the relationship between RE performance and model size for various open-source models. To examine temporal trends, Figure 10 plots model performance against their release dates, where open-source models are shown as dots (with marker size indicating model scale) and proprietary models are shown as triangles. Overall, performance tends to rise with newer releases, particularly among proprietary

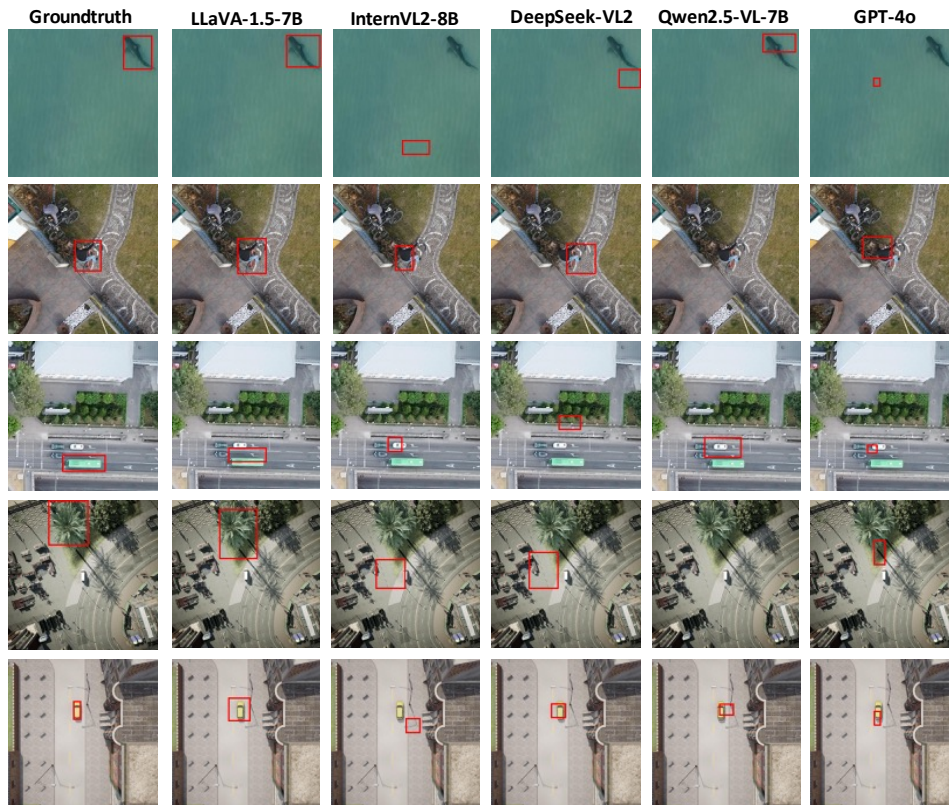


Figure 11: Grounding results from various models.

models such as GPT-5 and Gemini 2.5 Pro. Open-source models also progress over time, though less consistently: for instance, InternVL3.5, released after InternVL3, shows no clear RE improvement despite comparable size. A similar pattern appears in the Claude family, where later models (e.g., Claude 4.1 Opus) underperform earlier Sonnet versions on RE. These patterns indicate that top-down visual understanding is not a prioritized objective in current training regimes; most models appear to focus on mainstream capabilities such as chat, long-context reasoning, or coding, while robustness on top-down views receives little explicit attention. This highlights the underexplored status of top-down images and the importance of benchmarks like TDBench that bring this gap into focus.

## B.2 VISUAL GROUNDING

In TDBench, we employ a lenient criteria, centroid containment criterion, for visual grounding evaluation rather than the conventional Intersection over Union (IoU) metric typically used in object detection tasks. The reason is that aerial applications, such as drone navigation scenarios where precise object boundaries are less critical than accurate central positioning as waypoint. Specifically, a prediction is considered successful if the predicted object’s centroid falls within the ground truth bounding box, enabling effective target localization for hovering operations. While boundary precision is less relevant in many aerial contexts, we nevertheless present comparative performance analysis using both centroid containment and IoU thresholds in Table 4. Note that value of IoU here is obtained by the calculating the mean in 4 rotations dataset, whereas centroid performance is obtained under RE. We also show some examples of grounding results from some models in Figure 11 for reference.

## B.3 COMPREHENSIVE DIMENSION-WISE RESULTS

We have presented only aggregated performance summaries (Figure 1, Table 2 & 3) in previous sections. For completeness, Tables 5–8 provide the full dimension-wise results of all 60 evaluated

Table 4: Visual Grounding IoU vs Centroid Containment Comparison.

Metric	GPT 4o	GPT 4o mini	Gemini 1.5 pro	Gemini 1.5 flash	Claude 3.5 sonnet	Claude 3.5 haiku
Average IoU	0.05	0.03	<b>0.40</b>	0.25	0.07	0.06
Centroid Performance (%)	1.50	1.60	<b>36.40</b>	24.10	2.80	1.10

Metric	DeepSeek VL2-small	DeepSeek VL2-tiny	LLaVA-Next Qwen-7B	LLaVA-Next Qwen-0.5B	LLaVA 1.5-7B
Average IoU	0.09	0.08	0.06	0.05	<b>0.35</b>
Centroid Performance (%)	1.80	2.60	0.60	0.50	<b>36.50</b>

Metric	Qwen2.5 VL-7B	Qwen2.5 VL-3B	InternVL2 8B	InternVL2 4B	Phi4
Average IoU	0.07	0.02	0.04	0.02	0.01
Centroid Performance (%)	0.60	0.00	0.50	0.00	0.00

models (17 proprietary and 47 open-source) across the 10 evaluation dimensions in TDBench. Each table contains RE, VE,  $\theta$ ,  $r$ ,  $g$ , and  $A_{\text{adj}}$  for every model, with the best values highlighted in green and the worst in red (separately for open-source and proprietary models). Unlike the other three tables, Table 8 (Visual Grounding) presents only the top 12 models by  $A_{\text{adj}}$  in each group. Many models produced near-zero RE and consequently very low  $A_{\text{adj}}$  on this task, likely due to the lack of relevant training data, offering little comparative insight. In rare cases, such as for GPT-4o on *Scene Understanding*, a valid solution to the parameter system could not be found.

Table 5: VLMs in TDBench on Scene Understanding, Hallucination Detection, Object Presence.

Model	Scene Understanding						Hallucination Detection						Object Presence					
	RE	VE	$\theta$	r	g	$A_{adj}$	RE	VE	$\theta$	r	g	$A_{adj}$	RE	VE	$\theta$	r	g	$A_{adj}$
<i>Proprietary VLMs</i>																		
Claude 3.5 Haiku	0.740	0.864	0.853	0.965	0.278	0.823	0.835	0.901	0.884	0.986	0.260	0.871	0.390	0.601	0.627	0.888	0.119	0.557
Claude 3.5 Sonnet	0.775	0.899	0.896	0.964	0.338	0.863	0.635	0.828	0.855	0.928	0.234	0.794	0.430	0.650	0.640	0.905	0.197	0.579
Claude 3.7 Sonnet	0.780	0.892	0.861	0.975	0.384	0.839	0.745	0.881	0.907	0.952	0.189	0.864	0.325	0.537	0.530	0.885	0.146	0.469
Claude 4 Sonnet	0.745	0.865	0.885	0.958	0.150	0.848	0.600	0.796	0.772	0.938	0.315	0.724	0.330	0.534	0.525	0.890	0.140	0.467
Claude 4.1 Opus	0.800	0.899	0.896	0.972	0.266	0.871	0.515	0.743	0.742	0.912	0.254	0.677	0.340	0.550	0.526	0.896	0.165	0.472
GPT-4o-mini	0.870	0.934	0.940	0.981	0.197	0.922	0.745	0.875	0.846	0.968	0.365	0.819	0.465	0.635	0.642	0.923	0.120	0.592
GPT-4o	0.930	0.961	-	-	-	-	0.575	0.761	0.761	0.932	0.216	0.710	0.645	0.815	0.760	0.958	0.361	0.728
GPT-4.1 Nano	0.875	0.932	0.932	0.984	0.221	0.918	0.485	0.700	0.659	0.925	0.264	0.610	0.735	0.853	0.849	0.964	0.223	0.819
GPT-4.1	0.915	0.961	0.943	0.992	0.456	0.935	0.405	0.629	0.642	0.891	0.158	0.572	0.725	0.855	0.848	0.961	0.263	0.815
OpenAI o3	0.920	0.965	0.956	0.990	0.419	0.947	0.560	0.756	0.760	0.926	0.217	0.704	0.565	0.730	0.724	0.940	0.180	0.680
GPT-5 mini	0.920	0.949	0.951	0.992	0.116	0.943	0.185	0.388	0.431	0.809	0.068	0.349	0.865	0.919	0.906	0.988	0.249	0.895
GPT-5	0.930	0.971	0.973	0.989	0.344	0.962	0.550	0.730	0.707	0.939	0.226	0.664	0.615	0.754	0.731	0.958	0.201	0.700
Gemini 1.5 Flash	0.905	0.948	0.953	0.987	0.147	0.941	0.540	0.703	0.708	0.934	0.139	0.662	0.720	0.815	0.811	0.971	0.147	0.787
Gemini 1.5 Pro	0.920	0.953	0.956	0.991	0.134	0.947	0.525	0.714	0.719	0.924	0.175	0.664	0.810	0.886	0.882	0.979	0.193	0.864
Gemini 2.5 Flash-Lite	0.905	0.946	0.931	0.993	0.316	0.925	0.655	0.820	0.835	0.941	0.208	0.786	0.745	0.843	0.839	0.971	0.173	0.815
Gemini 2.5 Flash	0.920	0.956	0.953	0.991	0.249	0.945	0.590	0.784	0.729	0.947	0.345	0.690	0.770	0.866	0.875	0.969	0.151	0.847
Gemini 2.5 Pro	0.940	0.970	0.971	0.992	0.232	0.963	0.595	0.786	0.823	0.922	0.156	0.759	0.860	0.930	0.928	0.981	0.275	0.910
<i>Open Source VLMs</i>																		
Gemma3 4B	0.795	0.897	0.919	0.964	0.136	0.887	0.175	0.372	0.392	0.818	0.086	0.320	0.825	0.922	0.934	0.969	0.257	0.906
Gemma3 12B	0.780	0.896	0.907	0.963	0.246	0.873	0.255	0.477	0.477	0.855	0.134	0.407	0.805	0.894	0.894	0.974	0.216	0.871
Gemma3 27B	0.860	0.924	0.904	0.987	0.324	0.893	0.230	0.416	0.420	0.860	0.094	0.362	0.890	0.949	0.954	0.983	0.245	0.937
Deepseek VL2-Tiny	0.870	0.931	0.932	0.983	0.220	0.916	0.250	0.374	0.389	0.896	0.042	0.348	0.335	0.546	0.546	0.885	0.138	0.483
Deepseek VL2-Small	0.885	0.932	0.913	0.992	0.307	0.906	0.555	0.724	0.750	0.927	0.113	0.696	0.645	0.761	0.764	0.958	0.122	0.732
Deepseek VL2	0.840	0.925	0.929	0.975	0.272	0.906	0.560	0.755	0.780	0.921	0.169	0.718	0.695	0.771	0.772	0.974	0.085	0.752
InternVL2.5 4B-MPO	0.815	0.900	0.905	0.974	0.195	0.881	0.610	0.767	0.756	0.948	0.210	0.716	0.485	0.624	0.593	0.951	0.148	0.564
InternVL2.5 8B-MPO	0.810	0.881	0.848	0.988	0.284	0.838	0.625	0.785	0.809	0.937	0.139	0.758	0.415	0.594	0.573	0.922	0.153	0.528
InternVL3-1B	0.755	0.869	0.893	0.959	0.118	0.856	0.405	0.532	0.514	0.942	0.099	0.484	0.450	0.600	0.602	0.930	0.101	0.560
InternVL3-2B	0.855	0.922	0.917	0.983	0.259	0.901	0.365	0.519	0.524	0.914	0.084	0.479	0.615	0.749	0.743	0.954	0.157	0.708
InternVL3-8B	0.880	0.924	0.932	0.986	0.074	0.919	0.405	0.546	0.554	0.925	0.076	0.512	0.595	0.759	0.777	0.935	0.144	0.727
InternVL3-9B	0.830	0.916	0.927	0.973	0.199	0.902	0.415	0.613	0.624	0.903	0.131	0.563	0.485	0.656	0.646	0.931	0.156	0.601
InternVL3-14B	0.850	0.909	0.903	0.985	0.198	0.890	0.395	0.556	0.539	0.925	0.125	0.498	0.565	0.698	0.679	0.955	0.154	0.648
InternVL3-38B	0.950	0.976	0.982	0.992	0.140	0.974	0.520	0.654	0.620	0.957	0.159	0.593	0.645	0.770	0.782	0.953	0.112	0.746
InternVL3.5-1B	0.705	0.821	0.829	0.960	0.149	0.796	0.220	0.396	0.402	0.860	0.085	0.346	0.645	0.811	0.794	0.949	0.282	0.753
InternVL3.5-2B	0.750	0.845	0.848	0.970	0.148	0.823	0.140	0.273	0.286	0.837	0.047	0.239	0.780	0.879	0.896	0.966	0.129	0.865
InternVL3.5-4B	0.690	0.826	0.822	0.957	0.223	0.787	0.245	0.364	0.371	0.901	0.046	0.335	0.765	0.877	0.893	0.962	0.174	0.859
InternVL3.5-8B	0.700	0.834	0.819	0.961	0.258	0.787	0.130	0.275	0.307	0.807	0.040	0.247	0.720	0.839	0.791	0.976	0.319	0.772
InternVL3.5-14B	0.720	0.836	0.841	0.962	0.171	0.809	0.140	0.304	0.303	0.825	0.078	0.250	0.815	0.909	0.924	0.969	0.177	0.895
InternVL3.5-38B	0.855	0.921	0.938	0.977	0.077	0.916	0.380	0.569	0.568	0.904	0.128	0.513	0.730	0.866	0.860	0.959	0.293	0.825
InternVL3.5-1B-Thk	0.705	0.834	0.846	0.955	0.164	0.809	0.245	0.421	0.413	0.877	0.100	0.363	0.630	0.818	0.809	0.939	0.303	0.760
InternVL3.5-2B-Thk	0.720	0.820	0.807	0.972	0.185	0.784	0.230	0.502	0.559	0.801	0.125	0.448	0.545	0.767	0.808	0.906	0.185	0.732
InternVL3.5-4B-Thk	0.695	0.830	0.810	0.962	0.266	0.779	0.350	0.495	0.477	0.925	0.102	0.442	0.695	0.853	0.827	0.956	0.354	0.791
InternVL3.5-8B-Thk	0.700	0.839	0.826	0.959	0.268	0.792	0.240	0.436	0.459	0.850	0.084	0.391	0.715	0.834	0.814	0.968	0.246	0.788
InternVL3.5-14B-Thk	0.730	0.860	0.860	0.960	0.247	0.826	0.200	0.424	0.476	0.805	0.078	0.383	0.780	0.889	0.865	0.974	0.345	0.842
InternVL3.5-38B-Thk	0.880	0.930	0.934	0.985	0.146	0.920	0.435	0.629	0.616	0.916	0.167	0.565	0.695	0.853	0.885	0.941	0.168	0.833
VLM-R1-OVD	0.615	0.786	0.778	0.943	0.237	0.734	0.370	0.593	0.583	0.892	0.173	0.520	0.440	0.636	0.669	0.901	0.102	0.602
VLM-R1-Math	0.645	0.799	0.791	0.950	0.226	0.752	0.505	0.671	0.677	0.929	0.130	0.629	0.480	0.667	0.684	0.915	0.131	0.626
VLM-R1-REC	0.580	0.777	0.785	0.927	0.231	0.728	0.530	0.730	0.752	0.916	0.166	0.689	0.305	0.535	0.533	0.870	0.154	0.463
Kimi-VL-A3B-Thk	0.735	0.863	0.840	0.967	0.316	0.812	0.355	0.611	0.571	0.887	0.244	0.506	0.375	0.601	0.607	0.886	0.161	0.538
Kimi-VL-A3B-Instruct	0.850	0.926	0.908	0.983	0.365	0.893	0.625	0.761	0.764	0.951	0.147	0.727	0.630	0.746	0.745	0.959	0.124	0.715
Kimi-VL-A3B-Thk-2506	0.875	0.934	0.936	0.983	0.209	0.920	0.725	0.858	0.812	0.971	0.368	0.788	0.420	0.591	0.614	0.910	0.086	0.558
LLaVA-Interleave-Qwen-0.5B	0.710	0.797	0.792	0.973	0.128	0.771	0.205	0.334	0.345	0.878	0.047	0.303	0.460	0.604	0.584	0.942	0.128	0.550
LLaVA-1.5-7B	0.810	0.890	0.878	0.980	0.244	0.860	0.280	0.529	0.545	0.846	0.148	0.461	0.320	0.545	0.541	0.877	0.154	0.474
LLaVA-Next-Mistral-7B	0.820	0.896	0.889	0.980	0.225	0.871	0.585	0.704	0.710	0.953	0.095	0.676	0.755	0.836	0.842	0.973	0.109	0.819
LLaVA-Next-Vicuna-7B	0.720	0.829	0.819	0.968	0.198	0.793	0.340	0.481	0.496	0.910	0.059	0.452	0.520	0.701	0.711	0.925	0.151	0.658
LLaVA-Interleave-Qwen-7B	0.895	0.946	0.923	0.992	0.399	0.916	0.420	0.594	0.620	0.907	0.082	0.563	0.570	0.696	0.692	0.952	0.119	0.660
LLaVA-1.5-13B	0.760	0.873	0.874	0.966	0.227	0.844	0.450	0.620	0.659	0.909	0.061	0.599	0.620	0.776	0.774	0.946	0.195	0.732

Table 6: VLMs in TDBench on Object Localization, Attribute Recognition, Object Counting.

Model	Object Localization						Attribute Recognition						Object Counting					
	RE	VE	$\theta$	r	g	$A_{adj}$	RE	VE	$\theta$	r	g	$A_{adj}$	RE	VE	$\theta$	r	g	$A_{adj}$
<i>Proprietary VLMs</i>																		
Claude 3.5 Haiku	0.165	0.496	0.475	0.765	0.253	0.363	0.405	0.608	0.579	0.914	0.186	0.529	0.075	0.316	0.373	0.669	0.106	0.250
Claude 3.5 Sonnet	0.335	0.627	0.541	0.884	0.326	0.478	0.525	0.714	0.711	0.927	0.189	0.659	0.135	0.394	0.397	0.763	0.151	0.303
Claude 3.7 Sonnet	0.340	0.583	0.484	0.914	0.272	0.442	0.480	0.669	0.613	0.940	0.239	0.577	0.115	0.354	0.388	0.738	0.111	0.286
Claude 4 Sonnet	0.420	0.693	0.664	0.890	0.302	0.591	0.490	0.704	0.737	0.903	0.146	0.665	0.100	0.399	0.427	0.695	0.178	0.297
Claude 4.1 Opus	0.365	0.641	0.623	0.874	0.257	0.544	0.505	0.703	0.717	0.916	0.161	0.657	0.165	0.398	0.425	0.789	0.108	0.335
GPT-4o-mini	0.075	0.468	0.488	0.613	0.328	0.299	0.480	0.693	0.659	0.923	0.246	0.609	0.175	0.366	0.303	0.871	0.146	0.264
GPT-4o	0.435	0.728	0.722	0.879	0.334	0.635	0.610	0.796	0.800	0.934	0.245	0.747	0.200	0.465	0.370	0.855	0.236	0.316
GPT-4.1 Nano	0.570	0.811	0.874	0.899	0.207	0.785	0.700	0.839	0.865	0.949	0.137	0.820	0.185	0.453	0.411	0.818	0.197	0.336
GPT-4.1	0.660	0.839	0.846	0.940	0.287	0.795	0.680	0.818	0.779	0.966	0.293	0.753	0.235	0.477	0.437	0.856	0.184	0.374
OpenAI o3	0.780	0.891	0.900	0.965	0.232	0.868	0.720	0.838	0.812	0.970	0.264	0.788	0.215	0.480	0.421	0.844	0.215	0.356
GPT-5 mini	0.575	0.826	0.831	0.910	0.414	0.756	0.700	0.821	0.827	0.959	0.163	0.793	0.215	0.484	0.449	0.831	0.201	0.373
GPT-5	0.770	0.887	0.886	0.965	0.284	0.855	0.700	0.838	0.841	0.955	0.217	0.803	0.190	0.465	0.436	0.812	0.197	0.354
Gemini 1.5 Flash	0.600	0.841	0.926	0.897	0.144	0.831	0.780	0.869	0.861	0.975	0.207	0.840	0.255	0.494	0.506	0.842	0.136	0.426
Gemini 1.5 Pro	0.715	0.892	0.928	0.937	0.325	0.869	0.740	0.860	0.851	0.966	0.259	0.821	0.285	0.492	0.448	0.893	0.168	0.400
Gemini 2.5 Flash-Lite	0.460	0.721	0.744	0.886	0.241	0.660	0.695	0.819	0.792	0.968	0.252	0.766	0.125	0.374	0.376	0.759	0.142	0.285
Gemini 2.5 Flash	0.585	0.795	0.685	0.956	0.445	0.655	0.755	0.856	0.834	0.975	0.259	0.813	0.145	0.432	0.422	0.765	0.190	0.323
Gemini 2.5 Pro	0.780	0.901	0.900	0.964	0.331	0.868	0.805	0.900	0.913	0.969	0.177	0.885	0.210	0.499	0.483	0.811	0.207	0.392
<i>Open Source VLMs</i>																		
Gemma3 4B	0.035	0.400	0.074	0.684	0.377	0.051	0.435	0.677	0.698	0.888	0.190	0.620	0.035	0.301	0.281	0.590	0.188	0.166
Gemma3 12B	0.280	0.593	0.453	0.880	0.355	0.399	0.290	0.666	0.867	0.761	0.053	0.659	0.130	0.414	0.438	0.738	0.161	0.323
Gemma3 27B	0.440	0.689	0.646	0.907	0.290	0.586	0.590	0.770	0.757	0.939	0.242	0.711	0.125	0.365	0.363	0.766	0.137	0.278
Deepseek VL2-Tiny	0.130	0.410	0.395	0.756	0.184	0.299	0.610	0.774	0.789	0.938	0.160	0.740	0.165	0.369	0.319	0.848	0.145	0.220
Deepseek VL2-Small	0.375	0.705	0.697	0.853	0.364	0.595	0.725	0.831	0.835	0.965	0.153	0.806	0.235	0.395	0.361	0.898	0.110	0.325
Deepseek VL2	0.365	0.723	0.820	0.816	0.297	0.669	0.680	0.830	0.857	0.944	0.150	0.809	0.235	0.398	0.358	0.900	0.117	0.322
InternVL2.5 4B-MPO	0.180	0.531	0.363	0.826	0.363	0.300	0.570	0.754	0.741	0.936	0.233	0.693	0.260	0.432	0.415	0.890	0.108	0.369
InternVL2.5 8B-MPO	0.390	0.649	0.616	0.891	0.261	0.549	0.630	0.784	0.781	0.948	0.199	0.740	0.230	0.434	0.443	0.849	0.103	0.376
InternVL3-1B	0.110	0.459	0.441	0.702	0.267	0.309	0.500	0.699	0.696	0.921	0.192	0.640	0.300	0.427	0.446	0.906	0.043	0.404
InternVL3-2B	0.270	0.534	0.502	0.856	0.209	0.430	0.595	0.761	0.741	0.946	0.233	0.701	0.285	0.435	0.448	0.893	0.063	0.400
InternVL3-8B	0.570	0.769	0.724	0.941	0.317	0.681	0.660	0.807	0.820	0.947	0.171	0.777	0.165	0.414	0.454	0.776	0.113	0.352
InternVL3-9B	0.640	0.815	0.767	0.954	0.356	0.732	0.630	0.794	0.789	0.945	0.228	0.746	0.315	0.465	0.454	0.913	0.093	0.414
InternVL3-14B	0.595	0.823	0.883	0.906	0.191	0.800	0.650	0.792	0.783	0.954	0.209	0.747	0.320	0.490	0.496	0.896	0.091	0.444
InternVL3-38B	0.795	0.911	0.907	0.967	0.366	0.877	0.800	0.874	0.860	0.982	0.208	0.845	0.340	0.475	0.455	0.930	0.095	0.423
InternVL3.5-1B	0.330	0.588	0.566	0.873	0.215	0.494	0.540	0.703	0.729	0.928	0.098	0.676	0.360	0.482	0.479	0.931	0.070	0.446
InternVL3.5-2B	0.410	0.679	0.567	0.918	0.366	0.520	0.525	0.730	0.715	0.925	0.240	0.662	0.315	0.474	0.474	0.903	0.087	0.428
InternVL3.5-4B	0.625	0.815	0.805	0.938	0.307	0.755	0.555	0.720	0.716	0.938	0.170	0.672	0.280	0.487	0.478	0.875	0.133	0.418
InternVL3.5-8B	0.730	0.875	0.881	0.954	0.291	0.840	0.540	0.733	0.734	0.926	0.198	0.680	0.320	0.504	0.478	0.904	0.137	0.432
InternVL3.5-14B	0.710	0.874	0.899	0.943	0.262	0.847	0.515	0.709	0.697	0.927	0.207	0.646	0.300	0.499	0.523	0.870	0.092	0.455
InternVL3.5-38B	0.820	0.919	0.935	0.968	0.211	0.905	0.495	0.713	0.724	0.909	0.197	0.658	0.355	0.564	0.533	0.903	0.176	0.481
InternVL3.5-1B-Thk	0.210	0.459	0.447	0.827	0.160	0.370	0.525	0.693	0.704	0.929	0.130	0.654	0.185	0.429	0.379	0.835	0.181	0.316
InternVL3.5-2B-Thk	0.245	0.532	0.405	0.878	0.297	0.356	0.435	0.679	0.711	0.884	0.174	0.628	0.185	0.444	0.450	0.801	0.152	0.360
InternVL3.5-4B-Thk	0.525	0.781	0.814	0.896	0.280	0.729	0.555	0.734	0.723	0.936	0.206	0.677	0.175	0.451	0.477	0.778	0.153	0.371
InternVL3.5-8B-Thk	0.670	0.853	0.861	0.939	0.319	0.808	0.570	0.761	0.789	0.922	0.160	0.728	0.260	0.510	0.529	0.837	0.142	0.443
InternVL3.5-14B-Thk	0.650	0.853	0.805	0.944	0.474	0.760	0.570	0.748	0.760	0.931	0.168	0.707	0.325	0.539	0.513	0.892	0.167	0.458
InternVL3.5-38B-Thk	0.790	0.901	0.914	0.964	0.231	0.882	0.555	0.761	0.742	0.929	0.279	0.689	0.325	0.545	0.527	0.886	0.165	0.467
VLM-R1-OVD	0.445	0.731	0.698	0.891	0.363	0.622	0.525	0.738	0.742	0.917	0.221	0.681	0.160	0.407	0.416	0.787	0.137	0.328
VLM-R1-Math	0.495	0.772	0.668	0.920	0.476	0.614	0.585	0.764	0.759	0.937	0.218	0.711	0.145	0.367	0.347	0.804	0.136	0.279
VLM-R1-REC	0.330	0.641	0.561	0.871	0.347	0.489	0.455	0.711	0.752	0.882	0.193	0.663	0.120	0.354	0.298	0.796	0.166	0.237
Kimi-VL-A3B-Thk	0.160	0.455	0.330	0.830	0.271	0.274	0.555	0.749	0.749	0.928	0.216	0.694	0.060	0.368	0.423	0.612	0.188	0.259
Kimi-VL-A3B-Instruct	0.555	0.776	0.800	0.912	0.231	0.730	0.710	0.825	0.835	0.960	0.141	0.802	0.260	0.441	0.431	0.881	0.108	0.380
Kimi-VL-A3B-Thk-2506	0.510	0.746	0.686	0.926	0.353	0.635	0.650	0.806	0.793	0.951	0.252	0.754	0.120	0.331	0.327	0.778	0.114	0.254
LLaVA-Interleave-Qwen-0.5B	0.015	0.270	0.015	0.917	0.260	0.014	0.420	0.630	0.629	0.904	0.165	0.569	0.060	0.217	0.184	0.756	0.096	0.139
LLaVA-1.5-7B	0.115	0.535	0.733	0.627	0.282	0.460	0.385	0.644	0.638	0.881	0.226	0.562	0.180	0.361	0.359	0.842	0.093	0.302
LLaVA-Next-Mistral-7B	0.700	0.853	0.853	0.951	0.278	0.812	0.690	0.820	0.837	0.953	0.138	0.797	0.110	0.314	0.277	0.793	0.130	0.220
LLaVA-Next-Vicuna-7B	0.435	0.704	0.609	0.915	0.374	0.558	0.575	0.750	0.749	0.936	0.196	0.701	0.105	0.314	0.295	0.772	0.122	0.228
LLaVA-Interleave-Qwen-7B	0.170	0.514	0.472	0.771	0.284	0.364	0.660	0.807	0.813	0.949	0.191	0.772	0.175	0.351	0.322	0.858	0.110	0.277
LLaVA-1.5-13B	0.385	0.718	0.778	0.838	0.297	0.652	0.535	0.733	0.747	0.920	0.179	0.687	0.205	0.345	0.326	0.891	0.0	

Table 7: VLMs in TDBench on Attribute Comparison, Dynamic Temporal, Spatial Relationship.

Model	Attribute Comparison						Dynamic Temporal					Spatial Relationship						
	RE	VE	$\theta$	r	g	$A_{adj}$	RE	VE	$\theta$	r	g	$A_{adj}$	RE	VE	$\theta$	r	g	$A_{adj}$
<i>Proprietary VLMs</i>																		
Claude 3.5 Haiku	0.615	0.670	0.669	0.979	0.045	0.655	0.200	0.375	0.333	0.880	0.123	0.293	0.190	0.501	0.576	0.758	0.153	0.436
Claude 3.5 Sonnet	0.510	0.669	0.676	0.932	0.119	0.630	0.295	0.610	0.501	0.871	0.349	0.436	0.410	0.715	0.539	0.920	0.475	0.496
Claude 3.7 Sonnet	0.610	0.693	0.696	0.967	0.062	0.674	0.245	0.619	0.505	0.822	0.411	0.415	0.475	0.723	0.700	0.907	0.293	0.635
Claude 4 Sonnet	0.545	0.679	0.708	0.937	0.053	0.663	0.200	0.519	0.468	0.806	0.266	0.377	0.480	0.759	0.782	0.884	0.308	0.692
Claude 4.1 Opus	0.530	0.679	0.687	0.937	0.112	0.644	0.210	0.530	0.471	0.814	0.277	0.383	0.485	0.776	0.867	0.865	0.199	0.750
GPT-4o	0.420	0.630	0.660	0.893	0.119	0.590	0.145	0.432	0.383	0.783	0.215	0.300	0.025	0.393	0.983	0.399	0.004	0.392
GPT-4o	0.420	0.647	0.634	0.902	0.207	0.572	0.225	0.529	0.444	0.840	0.280	0.373	0.415	0.720	0.695	0.876	0.364	0.609
GPT-4.1 Nano	0.600	0.703	0.708	0.959	0.079	0.679	0.310	0.627	0.456	0.898	0.401	0.409	0.665	0.860	0.863	0.936	0.382	0.808
GPT-4.1	0.525	0.677	0.683	0.936	0.120	0.639	0.240	0.536	0.483	0.838	0.254	0.405	0.600	0.815	0.691	0.958	0.495	0.662
OpenAI o3	0.550	0.714	0.694	0.943	0.192	0.655	0.280	0.605	0.409	0.897	0.403	0.367	0.770	0.909	0.903	0.960	0.434	0.867
GPT-5 mini	0.540	0.705	0.710	0.934	0.145	0.663	0.210	0.481	0.413	0.843	0.227	0.348	0.855	0.934	0.951	0.974	0.153	0.926
GPT-5	0.580	0.733	0.731	0.944	0.158	0.690	0.340	0.679	0.324	0.966	0.541	0.313	0.805	0.922	0.958	0.957	0.119	0.918
Gemini 1.5 Flash	0.475	0.649	0.671	0.917	0.101	0.616	0.190	0.489	0.440	0.809	0.237	0.356	0.635	0.829	0.819	0.938	0.337	0.768
Gemini 1.5 Pro	0.565	0.704	0.696	0.949	0.142	0.661	0.185	0.469	0.485	0.785	0.170	0.381	0.620	0.845	0.857	0.921	0.388	0.790
Gemini 2.5 Flash-Lite	0.410	0.639	0.656	0.889	0.162	0.583	0.170	0.505	0.455	0.778	0.277	0.354	0.620	0.846	0.865	0.919	0.380	0.795
Gemini 2.5 Flash	0.455	0.691	0.663	0.909	0.262	0.603	0.225	0.525	0.515	0.812	0.220	0.418	0.820	0.921	0.943	0.966	0.186	0.911
Gemini 2.5 Pro	0.575	0.744	0.743	0.938	0.182	0.697	0.240	0.535	0.542	0.815	0.203	0.442	0.825	0.925	0.943	0.967	0.231	0.912
<i>Open Source VLMs</i>																		
Gemma3 4B	0.260	0.550	0.523	0.838	0.233	0.439	0.140	0.429	0.463	0.741	0.160	0.343	0.020	0.331	0.567	0.429	0.203	0.243
Gemma3 12B	0.450	0.634	0.610	0.927	0.176	0.565	0.165	0.415	0.472	0.769	0.098	0.363	0.135	0.550	0.816	0.638	0.162	0.520
Gemma3 27B	0.490	0.676	0.670	0.925	0.172	0.619	0.145	0.386	0.422	0.766	0.109	0.323	0.495	0.744	0.673	0.923	0.375	0.621
Deepseek VL2-Tiny	0.330	0.603	0.607	0.858	0.208	0.521	0.085	0.350	0.284	0.737	0.196	0.209	0.085	0.463	0.675	0.595	0.187	0.402
Deepseek VL2-Small	0.560	0.666	0.678	0.953	0.061	0.647	0.150	0.471	0.474	0.749	0.222	0.354	0.325	0.650	0.726	0.818	0.205	0.594
Deepseek VL2	0.595	0.669	0.672	0.970	0.052	0.652	0.155	0.444	0.389	0.793	0.222	0.308	0.345	0.665	0.593	0.868	0.368	0.515
InternVL2.5 4B-MPO	0.415	0.637	0.638	0.898	0.178	0.573	0.145	0.405	0.375	0.788	0.175	0.296	0.140	0.566	0.871	0.633	0.115	0.551
InternVL2.5 8B-MPO	0.455	0.593	0.596	0.935	0.088	0.557	0.195	0.497	0.500	0.789	0.206	0.395	0.440	0.740	0.662	0.897	0.433	0.594
InternVL3-1B	0.370	0.546	0.533	0.913	0.128	0.486	0.120	0.360	0.423	0.730	0.089	0.309	0.010	0.338	-	-	-	-
InternVL3-2B	0.420	0.645	0.665	0.891	0.156	0.593	0.135	0.380	0.419	0.753	0.111	0.316	0.140	0.534	0.255	0.815	0.437	0.208
InternVL3-8B	0.420	0.584	0.579	0.923	0.118	0.534	0.160	0.411	0.440	0.777	0.125	0.341	0.505	0.772	0.697	0.917	0.439	0.639
InternVL3-9B	0.450	0.649	0.669	0.906	0.130	0.606	0.145	0.401	0.476	0.743	0.091	0.354	0.595	0.807	0.813	0.924	0.300	0.751
InternVL3-14B	0.525	0.652	0.654	0.947	0.097	0.619	0.150	0.436	0.439	0.764	0.180	0.335	0.585	0.820	0.805	0.921	0.402	0.742
InternVL3-38B	0.635	0.728	0.733	0.965	0.075	0.707	0.190	0.453	0.450	0.806	0.163	0.363	0.720	0.875	0.921	0.965	0.462	0.793
InternVL3.5-1B	0.335	0.516	0.517	0.897	0.109	0.464	0.075	0.352	0.482	0.628	0.096	0.303	0.150	0.497	0.562	0.718	0.215	0.404
InternVL3.5-2B	0.295	0.540	0.542	0.859	0.163	0.465	0.155	0.393	0.452	0.765	0.085	0.346	0.365	0.642	0.653	0.864	0.226	0.564
InternVL3.5-4B	0.440	0.556	0.544	0.948	0.088	0.516	0.165	0.443	0.513	0.753	0.116	0.386	0.435	0.714	0.751	0.872	0.236	0.655
InternVL3.5-8B	0.395	0.554	0.531	0.928	0.129	0.493	0.135	0.398	0.440	0.744	0.125	0.328	0.495	0.752	0.721	0.908	0.349	0.655
InternVL3.5-14B	0.495	0.615	0.592	0.956	0.120	0.566	0.150	0.421	0.474	0.750	0.125	0.355	0.570	0.801	0.846	0.906	0.228	0.766
InternVL3.5-38B	0.440	0.621	0.607	0.922	0.155	0.560	0.205	0.440	0.438	0.827	0.138	0.362	0.660	0.856	0.811	0.947	0.469	0.767
InternVL3.5-1B-Thk	0.365	0.596	0.541	0.905	0.232	0.490	0.060	0.347	0.529	0.580	0.086	0.307	0.055	0.417	0.666	0.535	0.183	0.356
InternVL3.5-2B-Thk	0.255	0.586	0.571	0.815	0.282	0.465	0.065	0.345	0.463	0.612	0.115	0.283	0.225	0.591	0.515	0.805	0.364	0.414
InternVL3.5-4B-Thk	0.345	0.551	0.551	0.889	0.136	0.490	0.155	0.443	0.487	0.751	0.150	0.366	0.340	0.671	0.650	0.847	0.345	0.550
InternVL3.5-8B-Thk	0.320	0.578	0.529	0.881	0.237	0.466	0.115	0.399	0.472	0.702	0.127	0.332	0.435	0.725	0.681	0.891	0.371	0.606
InternVL3.5-14B-Thk	0.440	0.635	0.624	0.916	0.168	0.572	0.145	0.420	0.490	0.738	0.115	0.361	0.520	0.789	0.842	0.886	0.270	0.746
InternVL3.5-38B-Thk	0.410	0.629	0.622	0.901	0.181	0.560	0.215	0.460	0.452	0.830	0.155	0.375	0.640	0.850	0.874	0.924	0.332	0.808
VLM-R1-OVD	0.200	0.509	0.544	0.778	0.188	0.423	0.120	0.420	0.535	0.688	0.111	0.368	0.270	0.621	0.620	0.810	0.314	0.502
VLM-R1-Math	0.335	0.556	0.560	0.879	0.145	0.492	0.145	0.426	0.518	0.727	0.103	0.376	0.320	0.649	0.706	0.820	0.238	0.579
VLM-R1-REC	0.390	0.611	0.641	0.883	0.125	0.566	0.105	0.404	0.538	0.665	0.100	0.358	0.205	0.593	0.583	0.764	0.353	0.446
Kimi-VL-A3B-Thk	0.305	0.633	0.537	0.862	0.366	0.463	0.120	0.400	0.318	0.781	0.223	0.248	0.245	0.621	0.318	0.896	0.493	0.285
Kimi-VL-A3B-Instruct	0.370	0.545	0.540	0.910	0.117	0.491	0.120	0.379	0.355	0.762	0.168	0.270	0.425	0.682	0.703	0.881	0.211	0.620
Kimi-VL-A3B-Thk-2506	0.390	0.576	0.595	0.900	0.100	0.536	0.180	0.484	0.313	0.863	0.311	0.270	0.450	0.719	0.640	0.912	0.375	0.584
LLaVA-Interleave-Qwen-0.5B	0.660	0.672	0.675	0.994	0.004	0.671	0.135	0.312	0.278	0.835	0.112	0.232	0.005	0.233	0.030	0.545	0.223	0.016
LLaVA-1.5-7B	0.635	0.662	0.659	0.991	0.027	0.653	0.090	0.356	0.400	0.688	0.135	0.275	0.040	0.366	-	-	-	-
LLaVA-Next-Mistral-7B	0.560	0.670	0.668	0.957	0.093	0.639	0.125	0.362	0.428	0.735	0.084	0.314	0.175	0.566	0.519	0.753	0.365	0.390
LLaVA-Next-Vicuna-7B	0.655	0.675	0.669	0.995	0.028	0.666	0.145	0.372	0.415	0.769	0.091	0.319	0.080	0.482	0.095	0.825	0.447	0.078
LLaVA-Interleave-Qwen-7B	0.490	0.647	0.615	0.945	0.173	0.581	0.155	0.394	0.437	0.772	0.100	0.337	0.020	0.360	0.719	0.403	0.251	0.290
LLaVA-1.5-13B	0.495	0.620	0.605	0.951	0.112	0.576	0.120	0.393	0.461	0.714	0.118	0.329	0.090	0.458	0.563	0.630	0.235	0.355
LLaVA-Next-Vicuna-13B																		